Azole-Based Indoleamine 2,3-Dioxygenase 1 (IDO1) Inhibitors

Ute F. Röhrig,* Somi Reddy Majjigapu, Aline Reynaud, Florence Pojer, Nahzli Dilek, Patrick Reichenbach, Kelly Ascencao, Melita Irving, George Coukos, Pierre Vogel, Olivier Michielin,* and Vincent Zoete*
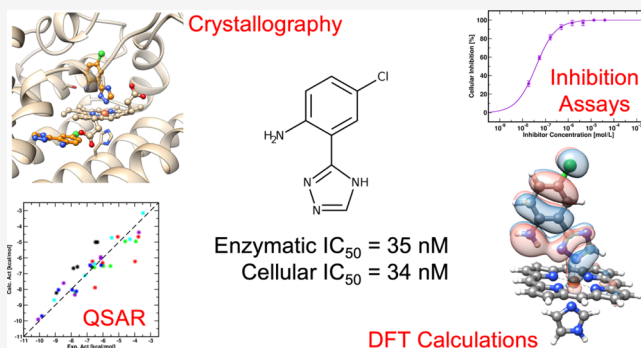
ACCESS | Metrics & More | Article Recommendations | Supporting Information

ABSTRACT: The heme enzyme indoleamine 2,3-dioxygenase 1 (IDO1) plays an essential role in immunity, neuronal function, and aging through catalysis of the rate-limiting step in the kynurenine pathway of tryptophan metabolism. Many IDO1 inhibitors with different chemotypes have been developed, mainly targeted for use in anti-cancer immunotherapy. Lead optimization of direct heme iron-binding inhibitors has proven difficult due to the remarkable selectivity and sensitivity of the heme—ligand interactions. Here, we present experimental data for a set of closely related small azole compounds with more than 4 orders of magnitude differences in their inhibitory activities, ranging from millimolar to nanomolar levels. We investigate and rationalize their activities based on structural data, molecular dynamics simulations, and density functional theory calculations. Our results not only expand the presently known four confirmed chemotypes of sub-micromolar heme binding IDO1 inhibitors by two additional scaffolds but also provide a model to predict the activities of novel scaffolds.

Crystallography · Inhibition Assays · QSAR · DFT Calculations

Enzymatic IC$_{50}$ = 35 nM
Cellular IC$_{50}$ = 34 nM

1. INTRODUCTION

Recent developments in cancer immunotherapy have greatly improved the prognosis of cancer patients, but low response rates caused by tumoral immune resistance remain an unsolved issue. Tryptophan catabolism along the kynurenine pathway has emerged as an important mechanism in this field, motivating the development of small-molecule inhibitors of indoleamine 2,3-dioxygenase 1 (IDO1) and of tryptophan 2,3-dioxygenase (TDO), the enzymes catalyzing the rate-limiting step in this pathway. However, despite compelling pre-clinical and early clinical data, a phase 3 clinical trial (ECHO-301) of the IDO1 inhibitor epacadostat (INCB024360) in combination with pembrolizumab failed to increase the overall and progression-free survival when compared to pembrolizumab alone.[1,2] Potential reasons for the negative outcome of this clinical trial and possible solutions have been suggested, such as the use of more potent and more specific IDO1 inhibitors and the use of dual IDO1/TDO inhibitors in combination with intratumoral kynurenine level monitoring.[3] Alternative targeting of the downstream effector aryl hydrocarbon receptor (AHR)[4−6] or the AHR-activating enzyme IL4I1 has also been suggested.[7] Novel aspects of IDO1 biology have recently come to light and might influence its role as an anti-cancer target, such as its signaling activity,[8−10] regulation by heme availability,[11] nitrite reductase activity in hypoxic tissues,[12] involvement in the redox signaling pathways of hydrogen peroxide and singlet oxygen,[13] and activation by polysulfides.[14]

There is an ongoing interest for IDO1 inhibitors capable of modulating these different pathways and processes.

We have previously classified the available IDO1 inhibitors into four types according to their preferential binding and inhibition mechanism.[15] Type I inhibitors preferentially bind to oxygen-bound holoIDO1 (*e.g.*, 1-methyl-L-tryptophan), type II inhibitors to free ferrous holoIDO1 (*e.g.*, epacadostat), type III to free ferric holoIDO1 (*e.g.*, navoximod), and type IV to apoIDO1 (*e.g.*, linrodostat). Since L-trp competitive type I inhibitors display the same relatively low (micromolar) affinity for IDO1 as the substrate, and type IV inhibitors were for the first time described in 2018,[11,16] most of the inhibitor design efforts of the last 15 years concentrated on the heme—iron binding type II and type III inhibitors.

Lead optimization of these inhibitors has proven difficult in the past due to the remarkable selectivity and sensitivity of the heme—ligand interactions to changes in the electronic structure of the ligand and due to the small size of the distal heme pocket (pocket A, Figure 1).[17] In fact, there are only four confirmed chemotypes of sub-micromolar type II or type III
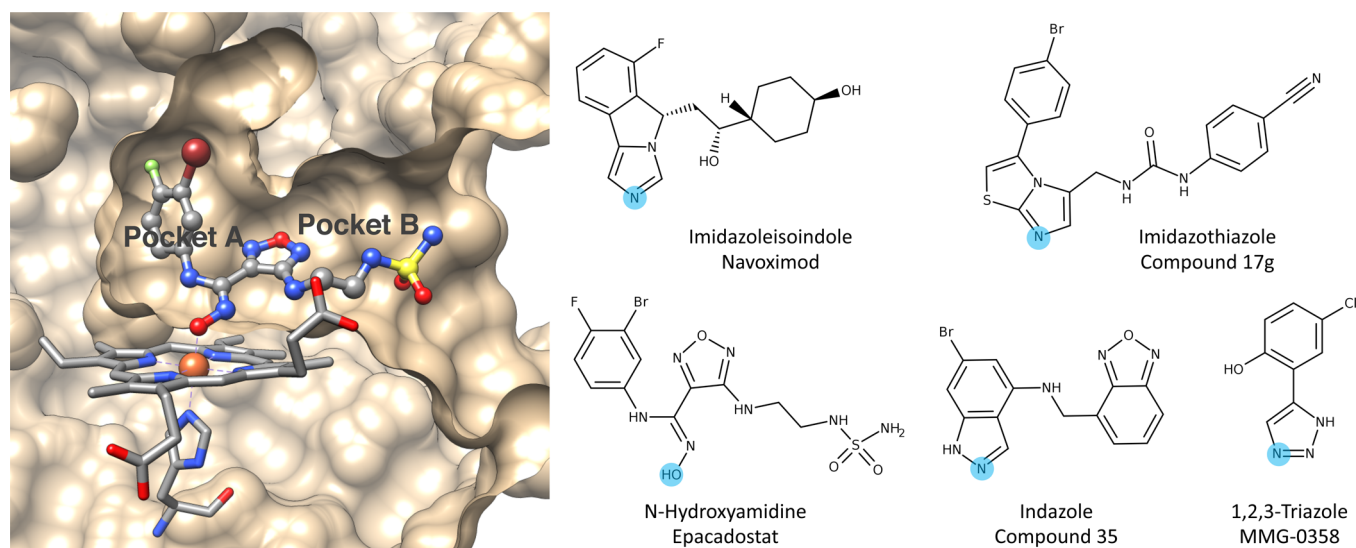
Figure 1. Binding pockets A and B in IDO1-active site (PDB ID 6e40; ligand: epacadostat) and examples of nanomolar inhibitors with different heme-binding scaffolds. The iron-binding atom, as confirmed by X-ray crystallography, is marked in blue.

IDO1 inhibitors, consisting of imidazoles, hydroxyamidines, indazoles, and 1,2,3-triazoles (Figure 1).

Imidazoles are classical heme binders, and 4-phenyl-imidazole is a known IDO1 ligand[18] and the first co-crystallized IDO1 inhibitor.[19] Structure-based optimization of this chemotype yielded the 2-hydroxy-substituted phenyl derivative (IC$_{50}$ 4.8 μM) as the most active compound.[20] Subsequent development also used pocket B (Figure 1) and led to the discovery of navoximod (Figure 1), first disclosed in the patent literature and more recently in the scientific literature.[21] Based on the pioneering work of New Link Genetics, other groups developed imidazole-based IDO1 inhibitors.[22−27] While there are very few examples of 4-phenylimidazoles of nanomolar potency, rigidification of the scaffold to imidazoleisoindole by a methylene linker fusing the N-1 of the imidazole with the 2′-position of the phenyl ring greatly improved the activity and ligand efficiency.[21] X-ray structures of IDO1 in complex with imidazoleisoindoles including navoximod have been reported (PDB IDs 5ek2, 5ek3, 5ek4, 6o3i).[21,22] Recently, two nanomolar 1-benzyl-imidazoles have also been described.[28] In the absence of structural data and *in vitro* inhibitory activities, the reported benzimidazole IDO1 inhibitors with low nanomolar activities in cellular assays[29] might in fact be apoIDO1 binding type IV inhibitors.

Providing a variation of the imidazole scaffold, nanomolar imidazothiazole-based IDO1 inhibitors were disclosed in 2014 by researchers from Sumitomo Dainippon Pharma, including both structural and functional data (Figure 1, compound 17g).[30] Subsequent works on this scaffold, however, showed that these compounds do not inhibit IDO1 in a cellular context.[31,32] Replacement of the phenyl ring in pocket A with a cyclopropylethynyl group and of the urea function by a thiourea function led to a compound with increased *in vitro* activity but still lacking cellular activity.[33]

The second high-affinity heme iron-binding scaffold, the *N*-hydroxyamidines including epacadostat (Figure 1), has been pioneered by researchers from Incyte.[34,35] Structural data (PDB IDs 5xe1, 5wn8, 6e40, 6e41, and 6pu7)[36−39] and quantum chemical computations[40] established that this scaffold binds through an oxygen atom to the heme iron,
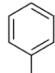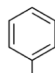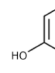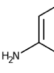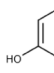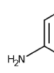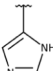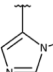
providing a hitherto unknown heme-binding group. In the following, many groups described *N*-hydroxyamidine derivatives as IDO1 inhibitors, modifying mainly the extension in pocket B and less frequently also the extension in pocket A.[39,41−45]

More recently, indazole has emerged as another potentially high-affinity heme-binding scaffold. In the patent literature, they were first described as TDO inhibitors, but over the last years, a few sub-micromolar IDO1 inhibitors have also been disclosed.[46−49] In addition, it has been suggested that they preferentially bind to ferrous IDO1[48] (type II inhibitors). This scaffold might provide a good route to dual IDO1/TDO inhibitors (Figure 1, compound 35).[49] Structural data is only available for an indazole bound to hTDO (PDB ID 6a4i) and reveals a direct N2−Fe bond.

Finally, we have previously discovered 1,2,3-triazole as a heme-binding scaffold yielding nanomolar IDO1 inhibitors.[17,50] The X-ray structure of the potent 4-phenyl-1,2,3-triazole MMG-0358 (PDB ID 6r63)[15] confirmed the predicted binding mode with a direct iron-1,2,3-triazole 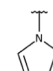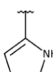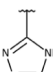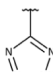bond. Such a bond also exists in the case of 4-amino-1,2,3-triazole bound to IDO1 (PDB ID 6f0a),[51] although this compound otherwise shows a different inhibition mechanism.[15] Recently, nanomolar 4,5-disubstituted 1,2,3-triazole IDO1 inhibitors occupying both pockets A and B have also been described without providing structural data.[52] In general, structural data of direct iron-1,2,3-triazole bonds is extremely scarce but has been documented for seviteronel binding to human cytochrome P450 17A1 (PDB ID 5irv).[53]

1,2,4-Triazole is a common heme-binding scaffold present in many antifungal drugs, and its direct iron binding in sterol 14α-demethylase (CYP51) is well documented by structural data. However, until now, efforts to develop IDO1 inhibitors based on this scaffold were unsuccessful. We demonstrated that imidazole antifungal drugs such as miconazole and sulconazole consistently inhibited IDO1 at micromolar levels, while all tested 1,2,4-triazole antifungals were inactive.[54] Bioisosteric replacement of imidazole by 1,2,4-triazole in 4-phenylimidazole also yielded an inactive compound.[50] The only known IDO1 inhibitor with a 1,2,4-triazole scaffold is the fused thiazolo-1,2,4-triazole Amg-1,[55] which has been co-

Table 1. Enzymatic IC$_{50}$ Values [μM] for rhIDO1 Inhibition, Mean of at Least Two Independent Assays[a]

	(a)	(b)	(c)	(d)	(e)	(f)
(1)	22 (3)	2.6 (0.2)	1.7 (0.1)	18 (2)	0.28 (0.02)	12.1 (0.3)
(2)	191 (2)	12.9 (0.4)	38 (1)	~1700[a]	17 (2)	~1200[a]
(3)	420 (30)	41 (2)	16 (3)	~1300[a]	2.1 (0.4)	88 (5)
(4)	10 (1)	0.35 (0.04)	2.3 (0.8)	33 (3)	0.059 (0.003)	1.5 (0.2)
(5)	~1800[a]	31 (4)	31 (1)	2.0 (0.7)	0.6 (0.1)	0.035 (0.004)
(6)	~2800[a]	100 (30)	700 (100)	5.8 (0.9)	16 (2)	0.22 (0.01)

[a]Standard deviations are given in parentheses. For more details, see the Supporting Information, Table S1. [b]Only one assay.

crystallized with IDO1 (PDB ID 4pk5)[30] and displays an activity in the low micromolar range.

There are very few examples of heme-binding tetrazoles in the literature. However, they have been exploited by Viamet Pharmaceuticals with the rationale to replace the imidazole or 1,2,4-triazole iron binding group in antifungals by a weaker iron-binding group in combination with potency-enhancing modifications in other parts of the compounds to achieve a better selectivity for CYP51B.[56,57] No nanomolar tetrazole IDO1 inhibitor has been reported to date.

Here, we report IDO1 enzymatic inhibition data for 36 closely related small heterocyclic compounds, including 12 known[17,20,21,50,54,58] and 24 new IDO1 ligands, spanning more than 4 orders of magnitude of activities on IDO1. They include the first nanomolar 1,2,4-triazole and tetrazole inhibitors. For the most active compounds, we determined cellular IC$_{50}$ and toxicity values. We provide three new X-ray structures of azole-bound IDO1 to support our structural hypotheses and rationalize the observed activities with the support of classical molecular dynamics (MD) simulations and static quantum mechanical (QM) calculations. The resulting model can be applied to predict activities of novel scaffolds and to meet the challenge of discovering novel high-affinity IDO1 inhibitor scaffolds.

2. RESULTS AND DISCUSSION

**2.1. Azole Compounds with Chloro-, Hydroxy-, and Amino-Substituted Phenyl Rings.** For the 4-phenyl-1,2,3-triazole scaffold, we have previously shown that introduction of two substituents on the phenyl ring, namely, 2-hydroxy and 5-chloro, improved the IC$_{50}$ values by more than 2 orders of

magnitude.[50] Here, we systematically investigated the influence of these two substitutions separately and in combination upon a series of six different heme-binding azoles. We added the 2-amino substitution and its combination with the 5-chloro substitution to the investigation because it showed a different influence upon inhibition activities than the 2-hydroxy substitution and led to some highly active compounds (Table 1). All compounds in Table 1, combining six different heme-binding azoles with six different phenyl ring substitutions, were bought or synthesized and tested for their IDO1 inhibitory activity. Surprisingly, they displayed activities ranging from 3 mM to 35 nM, spanning more than 4 orders of magnitude. Large activity differences are seen both between different azoles and between different phenyl ring substitutions. Interestingly, the influence of the phenyl ring substitutions and of the azole ring upon the activity depend on each other and show little correlation (Figure 2A,B).

We decided to look at this intriguing data set of highly similar small compounds with highly disparate activities in more detail with the aim to understand favorable and unfavorable factors for IDO1 inhibitory activity and to apply this knowledge to future inhibitor design.

2.2. Chemical Synthesis. The imidazole, triazole, and tetrazole derivatives were synthesized using the existing protocols or procedures adapted from the literature. Compounds 4a−4f have been described previously by us.[50] Other compounds were synthesized according to literature procedures [(1b, 1c, 1e),[20] (1d, 1f),[20,59] (2a−f),[59−61] (3c, 3e),[61,62] (3f),[62] (5b−c, 5e−g),[63] (6c, 6e−f),[64] 9,[65] 15,[66] 17,[67] 20,[68] 21,[69] and 23].[70] Briefly, the 4-phenylimidazole derivatives 1b−c and 1e were obtained by the reaction of α-
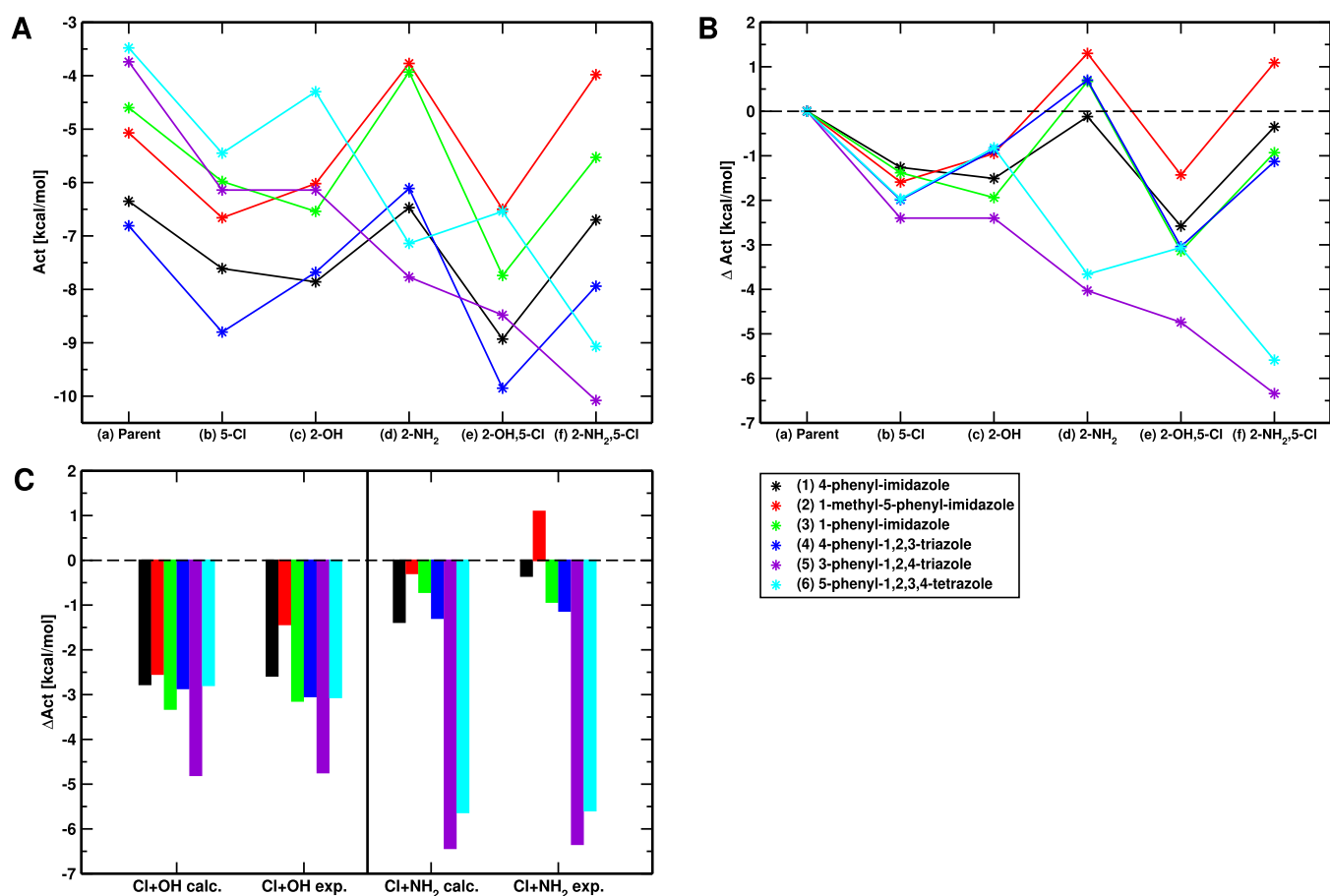
Figure 2. Experimentally determined enzymatic activities. The activity Act of each compound was calculated as $Act = -RT \ln IC_{50}$ in analogy to the relation between the binding free energy and measured K_i values. (A) Absolute activites. (B) Change in activities due to phenyl ring substitutions. (C) Additivity of substituent effects. Calc. stands for the calculated sum of substituent effects ($\Delta Act(Cl) + \Delta Act(OH/NH_2)$), while exp. stands for the experimentally measured effect of the di-substituted compounds ($\Delta Act(Cl + OH/NH_2)$). Left side: additivity of chloro/hydroxy effects; right side: additivity of chloro/amino effects.

Scheme 1[a]

36b: Ar = 3-Cl-C_6H_4, **36c**: Ar = 2-OH-C_6H_4,
36e: Ar = 2-OH-5-Cl-C_6H_3

1b: Ar = 3-Cl-C_6H_4, **1c**: Ar = 2-OH-C_6H_4,
1e: Ar = 2-OH-5-Cl-C_6H_3

37: Ar = 2-NO_2-C_6H_4,
38: Ar = 2-NO_2-5-Cl-C_6H_3

1d: Ar = 2-NH_2-C_6H_4,
1f: Ar = 2-NH_2-5-Cl-C_6H_3
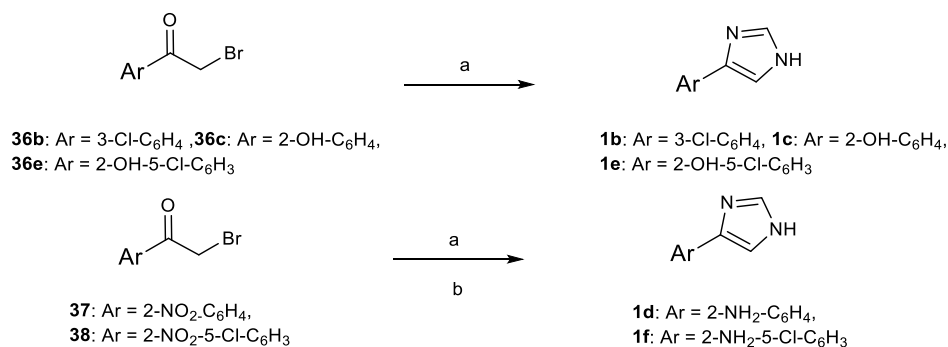
[a]Reagents and conditions: (a) formamide, 170−180 °C, rt, and 4 h and (b) $FeCl_3$, $N_2H_4 \cdot H_2O$, activated carbon, MeOH, rt−70 °C, and 48 h.

bromoketone derivatives (**36b−c**, **36e**) with formamide (Scheme 1). The amino derivatives **1d** and **1f** were obtained from the nitro arenes **37** and **38** through reaction with formamide, followed by reduction with $N_2H_4 \cdot H_2O/FeCl_3$ (Scheme 1). Compounds **2a** and **2b** were obtained by the reaction of the corresponding aryl iodides **39a** and **39b** with N-methyl imidazole in the presence of tricyclohexyl phosphonium tetrafluoroborate, Cs_2CO_3, and $Pd(OAc)_2$ in DMF at 120 °C. The same procedure applied to aryl iodides **42** and **43** produced the corresponding nitro derivatives that were then

reduced with $N_2H_4 \cdot H_2O/FeCl_3$ to produce **2d** and **2f**. Similarly, the corresponding aryl methyl ethers were obtained from aryl iodides **40** and **41**. Demethylation with 48% HBr in H_2O at 100 °C yielded compounds **2c** and **2e** (Scheme 2). Aryl iodide **39f** reacted with imidazole in the presence of N,N′-dimethylethylenediamine, Cs_2CO_3, and CuI in DMF at 140 °C to produce **3f**. In the same way, the aryl methyl ethers **40** and **41** were converted to the corresponding N-aryl imidazoles, followed by demethylation with 48% HBr in H_2O at 100 °C to produce phenols **3c** and **3e**, respectively (Scheme 3). The

Scheme 2[a]

39a: Ar = C_6H_5,
39b: Ar = 3-Cl-C_6H_4

40: Ar = 2-OMe-C_6H_4,
41: Ar = 2-OMe-5-Cl-C_6H_3

42 Ar = 2-NO_2-C_6H_4,
43: Ar = 2-NO_2-5-Cl-C_6H_3

2a: Ar = C_6H_5,
2b: Ar = 3-Cl-C_6H_4

2c: Ar = 2-OH-C_6H_4,
2e: Ar = 2-OH-5-Cl-C_6H_3

2d: Ar = 2-NH_2-C_6H_4,
2f: Ar = 2-NH_2-5-Cl-C_6H_3
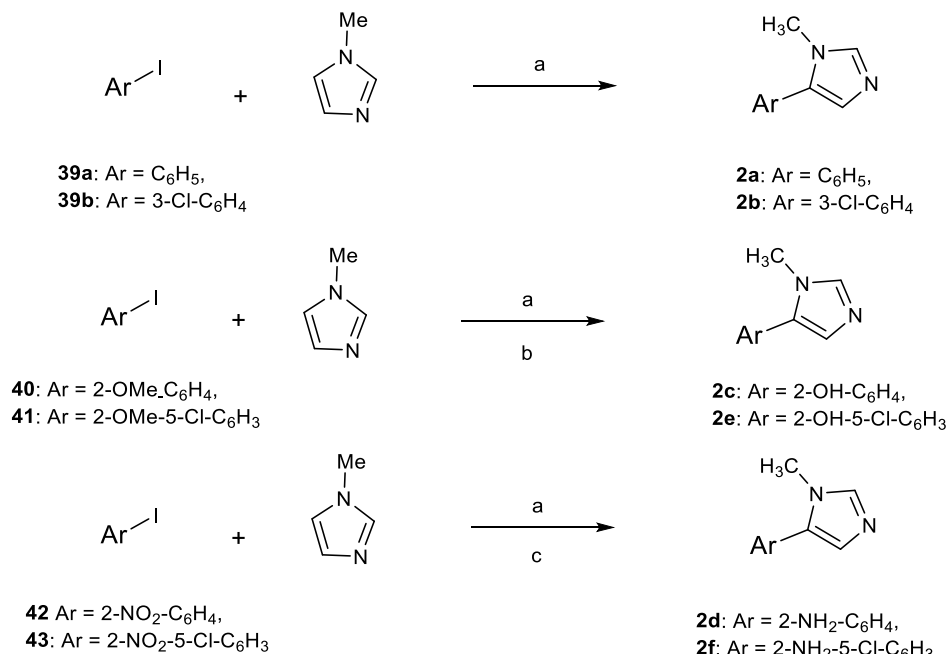
[a]Reagents and conditions: (a) tricyclohexylphosphonium tetrafluoroborate, Cs_2CO_3, Pd(OAc)$_2$, DMF, 120 °C, and 15 h; (b) 48% HBr in H_2O, 100 °C, and 14 h; and (C) $FeCl_3$, $N_2H_4 \cdot H_2O$, activated carbon, MeOH, rt–70 °C, and 48 h.

Scheme 3[a]

40: Ar = 2-OMe-C_6H_4,
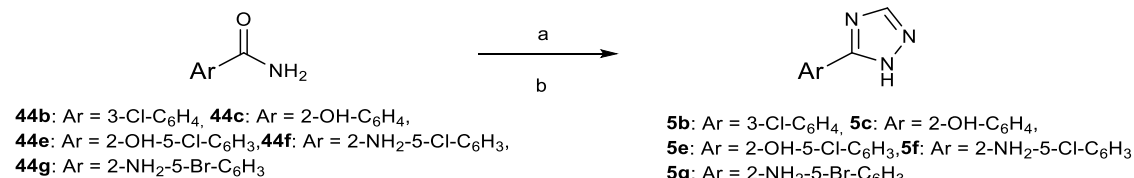**41**: Ar = 2-OMe-5-Cl-C_6H_3

39f: Ar = 2-NH_2-5-Cl-C_6H_3

3c: Ar = 2-OH-C_6H_4,
3e: Ar = 2-OH-5-Cl-C_6H_3

3f: Ar = 2-NH_2-5-Cl-C_6H_3
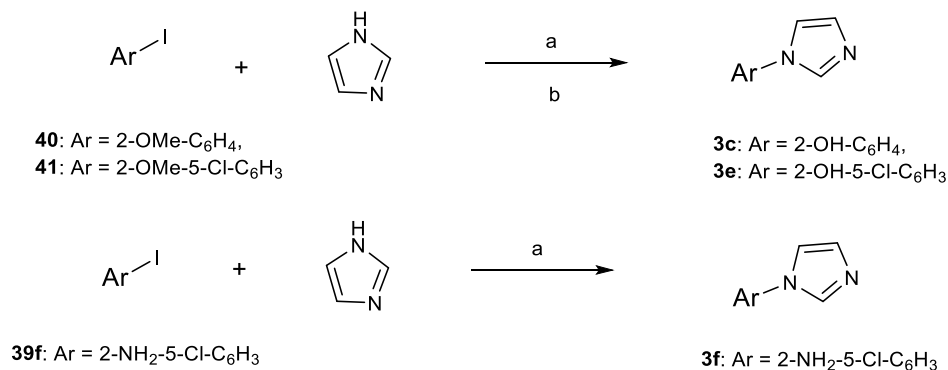
[a]Reagents and conditions: (a) N,N′-dimethylethylenediamine, Cs_2CO_3, CuI, DMF, 140 °C, and 12 h and (b) 48% HBr in H_2O, 100 °C, and 14 h.

Scheme 4[a]

Synthesis of 1H-1,2,4-triazoles derivatives:

44b: Ar = 3-Cl-C_6H_4, **44c**: Ar = 2-OH-C_6H_4,
44e: Ar = 2-OH-5-Cl-C_6H_3, **44f**: Ar = 2-NH_2-5-Cl-C_6H_3,
44g: Ar = 2-NH_2-5-Br-C_6H_3

5b: Ar = 3-Cl-C_6H_4, **5c**: Ar = 2-OH-C_6H_4,
5e: Ar = 2-OH-5-Cl-C_6H_3, **5f**: Ar = 2-NH_2-5-Cl-C_6H_3
5g: Ar = 2-NH_2-5-Br-C_6H_3

[a]Reagents and conditions: (a) N,N-dimethyl formamide-diethyl acetal (DMF-DMA), reflux, and 1 h and (b) $N_2H_4 \cdot H_2O$, AcOH, 90 °C, and 1.5 h.

triazoles **5b–c** and **5e–g** were obtained from benzamides **44b–c** and **44e–g** through condensation with N,N-dimethyl formamide-dimethyl acetal (DMF-DMA), followed by cyclization with hydrazine hydrate in acetic acid at 90 °C (Scheme 4). Tetrazoles **6c** and **6e–f** were prepared by reaction of the corresponding arene carbonitriles **45c** and **45e–f** with sodium

azide and triethylamine hydrochloride in toluene at 99 °C (Scheme 5).

Compound **9** was synthesized by N-arylation of pyrazole with phenyl iodide, pyrazole, and Cs_2CO_3 in DMF at 110 °C (Scheme 6). For compound **15**, phenylacetic acid underwent a double Vilsmeier–Haack reaction, followed by hydrolysis with NaOH and treatment with $SOCl_2$ in DCM to yield the

E

Scheme 5[a]

Synthesis of 1H-1,2,3,4-tetrazoles derivatives:

45c: Ar = 2-OH-C$_6$H$_4$,
45e: Ar = 2-OH-5-Cl-C$_6$H$_3$,
45f: Ar = 2-NH$_2$-5-Cl-C$_6$H$_3$

6c: Ar = 2-OH-C$_6$H$_4$,
6e: Ar = 2-OH-5-Cl-C$_6$H$_3$,
6f: Ar = 2-NH$_2$-5-Cl-C$_6$H$_3$
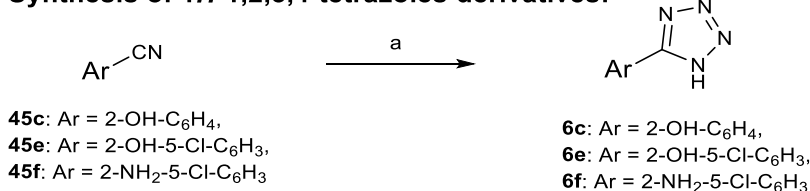
[a]Reagents and conditions: (a) NaN$_3$, Et$_3$N·HCl, toluene, rt–90 °C, and overnight.

Scheme 6[a]
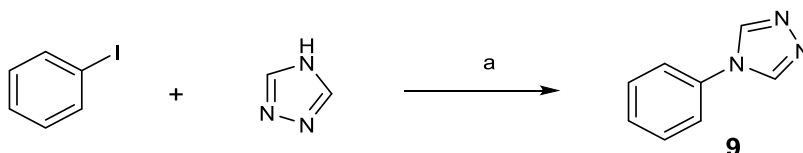
[a]Reagents and conditions: (a) Cu(OAc)$_2$·H$_2$O, Cs$_2$CO$_3$, DMF, 110 °C, and 24 h.

chloroacrolein, which was heated in DMF at 70 °C with NH$_4$SCN to yield compound **15** (Scheme 7). Compound **17**

Scheme 7[a]

[a]Reagents and conditions: (a) POCl$_3$, DMF, 85 °C, and 2 h; (b) NaOH, EtOH/H$_2$O, reflux, and 1 h; (c) SOCl$_2$, CH$_2$Cl$_2$, 0 °C, and 1 h; and (d) NH$_4$SCN, DMF, 70 °C, and 16 h.

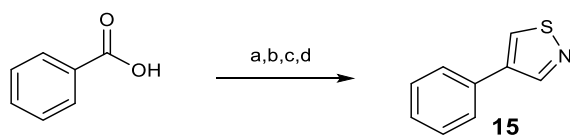was obtained from the treatment of methyl benzenecarbothioate with TMSCHN$_2$ and n-BuLi at −78 °C (Scheme 8). Compound **20** was synthesized by the coupling reaction of benzaldehyde with TosMIC in the presence of K$_2$CO$_3$ in MeOH (Scheme 9). The 4-phenylisoxazole **21** was obtained from 2-phenylmalonaldehyde and NH$_2$OH·HCl in EtOH at 80 °C (Scheme 10). Compound **23** was prepared by the reaction of benzohydrazide with triethyl orthoformate and p-TsOH in toluene at reflux (Scheme 11). Compounds **1a**, **3a**, **3b**, **3d**, **5a**, **5d**, **6a**, **6b**, **6d**, **22**, and **29** were bought from Sigma-Aldrich and compound **7** from Fluorochem.

2.3. Enzymatic Activities. The enzymatic IC$_{50}$ values were measured as previously described.[71] Briefly, ascorbate and methylene blue were used as reductants and catalase to remove hydrogen peroxide. Triton-X was added to inhibit compound aggregation, and a substrate concentration of 100 μM L-trp was chosen to minimize substrate inhibition. With an estimated IDO1 concentration of about 40 nM (2.5 μg/mL), an incubation time of 20 min at room temperature allowed for

stopping the reaction in its linear phase. Kynurenine and L-trp concentrations were determined by HPLC through UV detection. The measured IC$_{50}$ values are given in Table 1, while dose−response curves and Hill slopes can be found in the Supporting Information (Figure S1). We chose to test compounds at maximal concentrations of 1 mM to be able to also detect weak binders. The most active compound, **5f**, is a tight binder with the IC$_{50}$ value in the range of the enzyme concentration. We therefore determined its apparent K_i value using the Morrison equation.[72,73]

From Table 1 and Figure 2A,B, it is clear that for the unsubstituted parent compounds (**a**), the 1,2,3-triazole heterocycle is the most potent, the imidazoles are of intermediate activity, and the tetrazole performs the worst. The 5-chloro substitution (**b**) is favorable for all scaffolds and does not change this ordering. The 2-hydroxy substitution (**c**) is also favorable for all scaffolds, but in a more diverse way, changing also the ordering. This is even more strikingly the case for the 2-amino substitution (**d**), which is very favorable for the 1,2,4-triazole and the tetrazole but neutral or unfavorable for the other scaffolds. The combination of 2-hydroxy or 2-amino substitution with the 5-chloro substitution (Figure 2C) generally produces additive results, except for the 1-methyl-imidazole scaffold (red bar), where the effect of combining the two substituents is smaller than the sum of the effects of the single substituents. The strongest substitution effects are in all cases seen for the 1,2,4-triazole scaffold, yielding IC$_{50}$ values ranging from 1.8 mM to 35 nM, while the biggest dependence on the character of the azole ring was detected for the 2-amino-5-chloro substitution (IC$_{50}$ values of 1.2 mM to 35 nM).

Scheme 8[a]
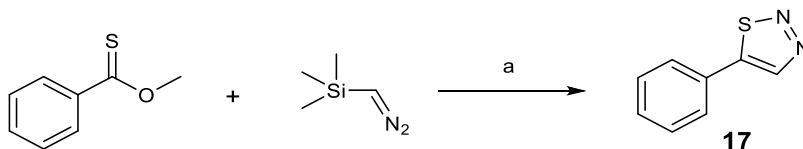
[a]Reagents and conditions: (a) n-BuLi, Et$_2$O/H$_2$O, -78 °C (30 min), 0 °C (30 min), and rt (1 h).

Scheme 9[a]
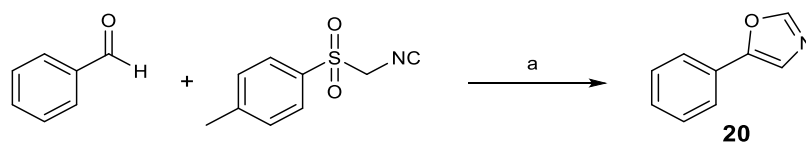
[a]Reagents and conditions: (a) K_2CO_3, MeOH, 80 °C, and 2 h.

Scheme 10[a]
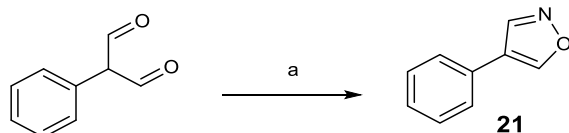
[a]Reagents and conditions: (a) $NH_2OH \cdot HCl$, EtOH, reflux, and 2 h.

In the following, we first describe the cellular activities of compounds **1a** to **5f** before rationalizing the observed enzymatic activities based on structural and theoretical data.

2.4. Cellular Activities. We tested the cellular hIDO1 inhibitory activity (Figure 3A) and toxicity (Figure 3B) of all active compounds at a concentration of 200 μM (Table S1) to be able to also detect weak cellular inhibitors. As some aniline compounds reacted with Ehrlich's reagent (p-dimethylamino-benzaldehyde, p-DMAB), the kynurenine content of these samples had to be determined by HPLC (Figure S3). In general, the compounds displayed very little cytotoxicity under the experimental conditions; only the amino-substituted 1,2,3-triazoles showed up to 30% of toxicity.

Cellular inhibition was observed to be closely related to enzymatic activity, showing a sigmoidal dependence (Figure 3C). The 1-phenyl-imidazole **3e** is an outlier of this dependence, showing much lower cellular activity than expected for an unknown reason. We proceeded to determine cellular IC_{50} values for the 10 most active compounds (Supporting Information, Table S1, Figure S2). Figure 3D shows the correlation between cellular and enzymatic activities, including our previously published cellular data for compounds **4a**, **4b**, and **4c**.[50] There is generally a good correlation, except for the tetrazole **6f**, which displays a 16 times higher enzymatic than cellular activity. This might be due to the presence of a negative charge on the tetrazole under physiological conditions, hampering cellular uptake. Compounds **1e** (0.88 ± 0.16 μM), **4b** (0.62 ± 0.01 μM),[50] **4e** (0.11 ± 0.04 μM), and **5f** (0.034 ± 0.011 μM) show nanomolar IC_{50} values also in the cellular assay (Figure 3E). In summary, the cellular assay data shows that most azoles are as active in the cellular environment as in the *in vitro* assay without significant toxicity, supporting their interest for drug development.

2.5. Structural Data for Azole Compounds. Structural data was available for three of the compounds, 4-phenyl-imidazole (compound **1a**, PDB ID 2d0t),[19] 4-(5-Cl-phenyl)-imidazole (compound **1b**, PDB ID 6e42),[38] and MMG-0358 (compound **4e**, PDB ID 6r63).[15] All the three compounds bind similarly to the heme iron of IDO1 through an azole ring nitrogen (Figure 4A−C).

The chloro substituent in the latter two is oriented toward a small hydrophobic cavity between Cys129, Leu234, and Gly262 (Figure 4B,C). The closest contact (3.2−3.4 Å) exists with the sulfur atom of Cys129 and is smaller than the sum of their van der Waals radii. However, the angle C−Cl⋯S of 95−112° is in disagreement with a halogen bond, where this angle should be close to 180° due to the σ-hole of the C−Cl bond.[74,75] Another contact exists between the chloro substituent and the backbone amide carbon of Gly262 (3.6 Å), forming a characteristic C=O⋯Cl angle of about 60°. This "side-on carbon interaction" between the electronegative belt around halogen atoms and the positively polarized amide carbon has been found in the crystallographic structures of different small molecules[76] and ligand−protein complexes.[77] Hydrophobic contacts, which are frequently observed for chlorine,[77] exist mainly between the Cl and the side chain of Leu234 (Figure 4C). Taking all evidence into account, we suggest that the chloro primarily interacts *via* van der Waals and dipolar interactions with the IDO1 binding pocket, in addition to modulating the electronic properties of the azole ring. This is at variance with earlier suggestions of a chlorine−cysteine halogen bond,[36] which are known to be extremely rare.[77]

The hydroxy group of MMG-0358 forms a hydrogen bond with the side chain of Ser167, probably donating the hydrogen, because the side chain of Ser167 simultaneously donates a hydrogen bond to the backbone oxygen of Phe163 (Figure 4C). The importance of this interaction has been demonstrated previously by the strongly increased IC_{50} value of compound **1c** in the Ser167Ala hIDO1 mutant (41 μM) as compared to the wild type (1.2 μM).[78]

Here, we co-crystallized compounds **4f** and **5f** with rhIDO1 and resolved the X-ray structures of the complexes. Additionally, we co-crystallized an analogue of **5f**, where the chloro substituent is replaced by a bromo substituent (**5g**). Compound **5g** showed an even better enzymatic IC_{50} value (0.020 ± 0.001 μM) than **5f**, and the bromo substituent is very amenable to X-ray crystallography because of its high electron density. The $2F_o − F_c$ maps of the bound ligands are shown in the Supporting Information (Figure S4).

Scheme 11[a]
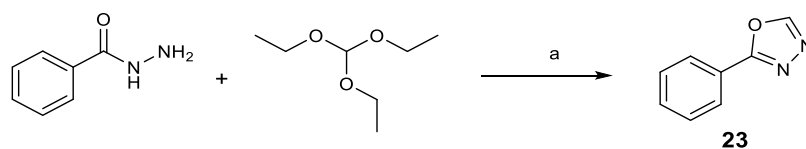
[a]Reagents and conditions: (a) p-TsOH, toluene, reflux, and 2 h.
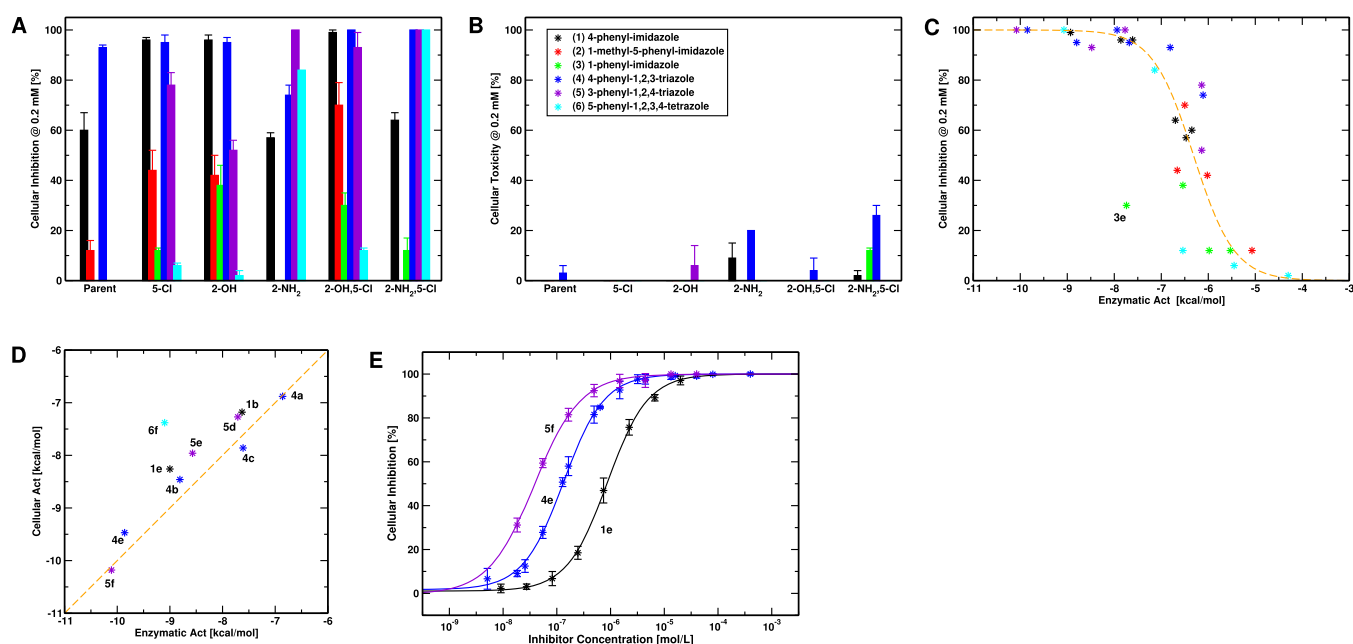
Figure 3. Cellular inhibition data and its comparison to enzymatic inhibition data. (A) Cellular inhibition of kynurenine production at a compound concentration of 200 μM. (B) Cellular toxicity under the same conditions. (C) Cellular inhibition compared to enzymatic activity. The orange line is a sigmoidal fit to all data points except for the outlier of compound **3e**. (D) Correlation between cellular activity and enzymatic activity. Color code given in the legend of part B. (E) Cellular dose−response curves of compounds **1e**, **4e**, and **5f**.

The 1,2,3-triazole **4f** (PDB ID 7ah4, Figure 4D) binds to IDO1 in the same way as **4e**, with the triazole ring directly bound to the heme iron, the chloro substituent in the hydrophobic cavity close to Cys129 (distance 3.4 Å) and Gly262 (distance 3.7 Å), and the amino instead of the hydroxy group making a hydrogen bond to Ser167 in the back of pocket A. The orientation and protonation state of the 1,2,3-triazole ring cannot be unequivocally determined from the electron density. In analogy to the structure of **4e**, the conformation shown in Figure 4D was selected based on the proximity between the N3 atom of the triazole ring and the backbone amide nitrogen of Ala264 (3.0 and 2.7 Å in chains A and B, respectively). In this conformation, the negatively charged triazole could make a favorable electrostatic interaction with the NH hydrogen. In both asymmetric subunits, a second ligand is bound to pocket D on the proximal heme side, roughly parallel to the heme plane. This ligand binding site, which has been observed by several groups since 2017,[15,37,38] is opened by a conformational change of Phe270, clearly seen here in the electron density. In the case of ligand **4f**, there seem to be two orientations of the ligand in pocket D present (Figure 4G), the slightly higher populated one (shown in magenta) similar to the one of compounds **4e** and **1b**, with the triazole pointing toward His346 and the chloro substituent toward a hydrophobic aliphatic pocket formed by Val170, Ala174, Leu207, and Ala210. The other ligand pose (dark green) is roughly rotated by 180°, with the phenyl ring pointing toward the heme and the chloro substituent toward His346. This ligand pose makes a hydrogen bonding interaction with Asp274 and Phe270 bridged by a solvent molecule.

Interestingly, the electrostatic potential created by the protein and the heme cofactor in pocket D is negative, regardless of the oxidation state of the heme iron (Figure 5). However, the electrostatic potential in pocket A strongly depends on the iron charge, being slightly positive in the case

of ferric heme but negative in the case of ferrous heme. This supports the earlier formulated hypothesis that the 1,2,3-triazoles bind in their deprotonated form to ferric heme. On the other hand, the ligands in pocket D are most likely present in their neutral form.

The X-ray structure of **5f** bound to IDO1 demonstrates that the 1,2,4-triazole binds very similar to pocket A as the 1,2,3-triazole (PDB ID 7ah5, Figure 4E) with the chloro substituent close to Cys129 and Gly262 and the amino group pointing to the back of pocket A. The amino group simultaneously donates two hydrogen bonds to Ser167 and to the N2 atom of the triazole ring. Compound **5f** is also detected in pocket D, adopting a distinct binding mode, with the phenyl ring pointing toward the heme, but at variance with compound **4f** pointing the chloro substituent toward Phe214 and the amino group toward Arg343 (Figure 4H).

Compound **5g** (PDB ID 7ah6) binds very similarly to pocket A as compound **5f**. The bromo substituent is located at a distance of 3.6 Å from the sulfur atom of Cys129 and at 3.5 Å from the backbone amide carbon of Gly262. Inside pocket D (Figure 4I), it adopts yet another binding mode, occupying the same plane but pointing the triazole toward Phe214 and the amino group toward the heme propionate donating a hydrogen bond to it (distance 2.8 Å).

In summary, ligands binding to pocket D all adopt a planar conformation with respect to the heme plane but can adopt different conformations inside this plane depending on the scaffold and the substituents. The halogen substituent is located either in a hydrophobic aliphatic pocket or close to the His346 or Phe214 aromatic rings. These interactions could contribute to ligand binding in pocket D, as the unsubstituted compound **1a** was not detected in this pocket. However, the absence of specific interactions suggests a low-affinity site potentially only accessible at the very high ligand concentrations used for crystallization.

H
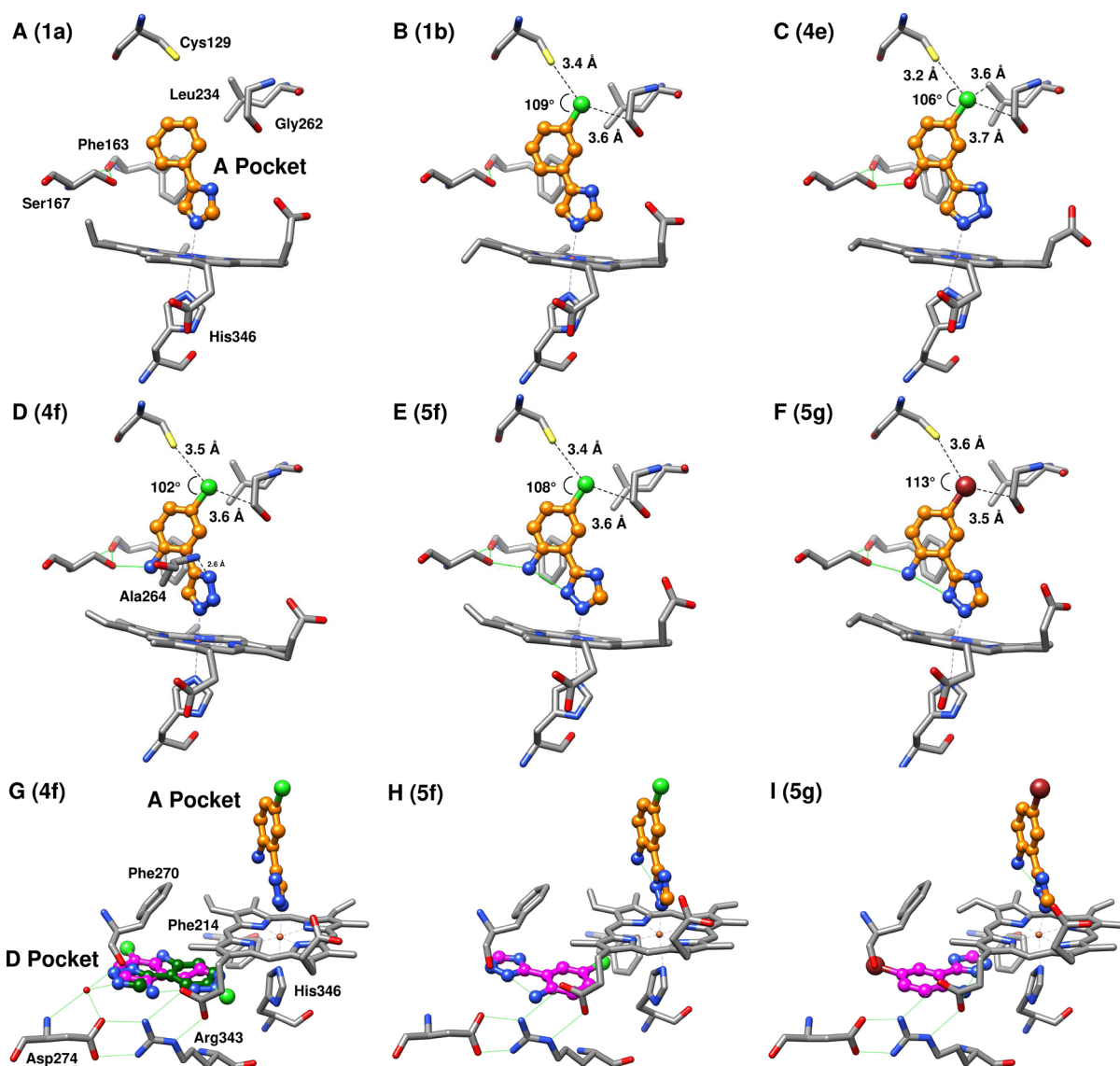
Figure 4. X-ray crystal structures of hIDO1 in complex with (A) compound **1a** (PDB ID 2d0t), (B) compound **1b** (PDB ID 6e42), (C) compound **4e** (PDB ID 6r63), (D,G) compound **4f** (PDB ID 7ah4), (E,H) compound **5f** (PDB ID 7ah5), and (F,I) compound **5g** (PDB ID 7ah6). The structures of **4f**, **5f**, and **5g** have been resolved for the present work. Ligand carbon atoms in pocket A are highlighted in orange, in pocket D in magenta/dark green. Hydrogen bonds are displayed as green lines. (A−F) Pocket A: Distances of halogen substituents with the closest protein contacts are indicated and the carbon−halogen−sulfur angle is given. (G−I) Ligand binding poses in pocket D are shown. For **4f**, two alternative conformations are detected and depicted in magenta and dark green, respectively.
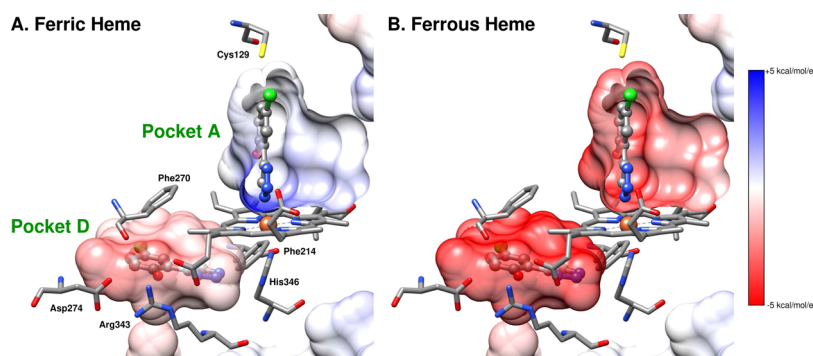
Figure 5. Electrostatic potential generated by the protein and the heme cofactor in pockets A and D of holoIDO1 (PDB ID 6r63). (A) Ferric heme. (B) Ferrous heme.

I
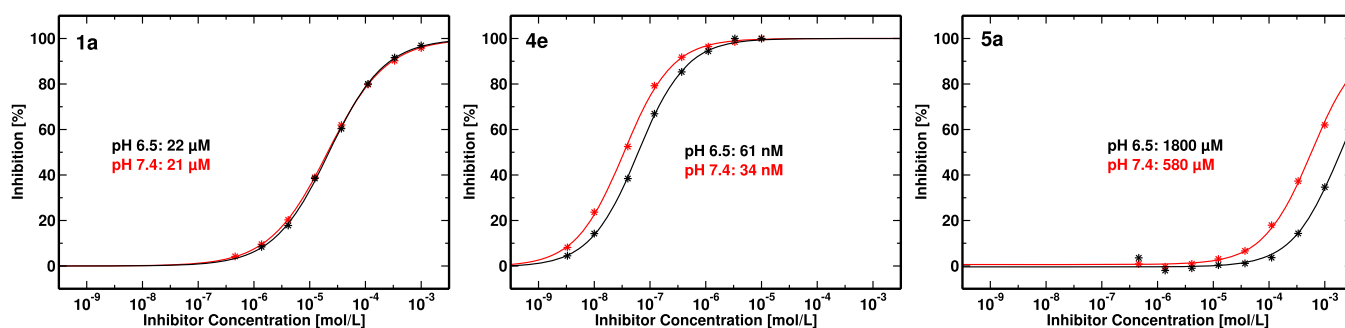
Figure 6. Enzymatic dose−response curves measured at different pH values for an imidazole (**1a**), a 1,2,3-triazole (**4e**), and a 1,2,4-triazole (**5a**). While the activity of the imidazole is pH-insensitive, both the 1,2,3-triazole and the 1,2,4-triazole are more active at higher pH.
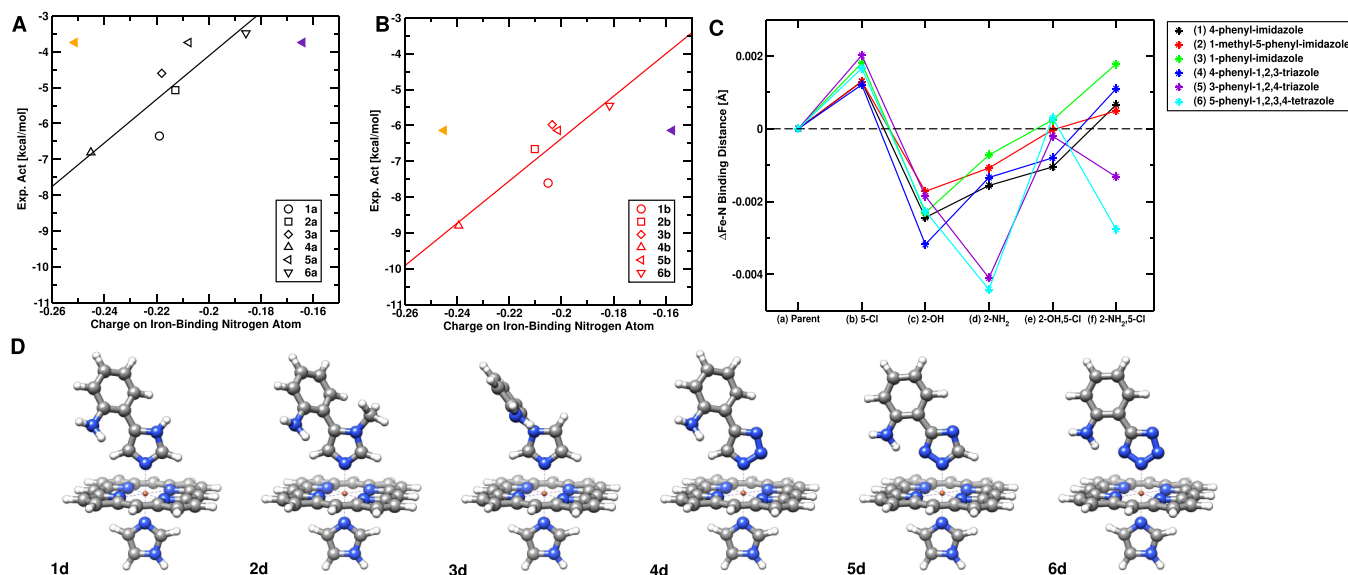
Figure 7. DFT calculations. (A) Correlation between the calculated Hirshfeld charge on the iron-binding nitrogen atom and the experimentally measured activity for unsubstituted parent compounds. For 1,2,4-triazole **5a**, the charges for the negatively charged compound (orange left triangle), for the neutral compound (purple left triangle), and their average (black left triangle) are shown. (B) The same correlation for *m*-chloro-substituted compounds (red). (C) Iron−nitrogen bond lengths in a ferric heme model system relative to the unsubstituted parent compounds. (D) Optimized geometries of 2-amino-substituted compounds in ferric heme models.

2.6. Protonation States of Active Species. It is known that ligand−protein binding,[79] and especially ligand binding to ferric hemoproteins,[80−82] induces large pK_a shifts in ligands. In our earlier works on 4-phenyl-1,2,3-triazole IDO1 inhibitors, we concluded that this scaffold most likely binds in its deprotonated, negatively charged form to the ferric heme cofactor.[50] More recently, we corroborated preferential binding of compounds **1a** and **4e** to ferric IDO1 by experimental techniques and reported density functional theory (DFT) calculations, suggesting that the deprotonation of compound **4e** is energetically much more favorable when bound to ferric heme than in solution.[15]

Here, we tested compounds **1a**, **4e**, and **5a** in the enzymatic assay at two different pH values, namely, at pH 6.5 and at pH 7.4 (Figure 6). We did not test other imidazoles for their pH dependence, as they can only bind to holoIDO1 in their neutral form. We also did not test the tetrazoles, as their low pK_a value in solution (4.53)[83] ensures their prevalent existence in their negatively charged form at physiological pH values. At both pH values, the enzymatic reaction is about equally efficient. While the IC_{50} value of imidazole **1a** remains constant, the IC_{50} of 1,2,3-triazole **4e** shifts to a lower value at higher pH, as shown previously.[50] The same is true for the

1,2,4-triazole **5a**, supporting the hypothesis that the 1,2,4-triazoles bind stronger to IDO1 in their deprotonated form.

In summary, our results suggest that the imidazoles bind in their neutral form to ferric holoIDO1, while the 1,2,3-triazoles and tetrazoles bind in their anionic form to it. The activity of the 1,2,4-triazole **5a** shows a pH dependence and is likely to bind to IDO1 in its deprotonated form.

2.7. Molecular Modeling. The activity of the azole compounds is determined by their binding free energies to holoIDO1, which are influenced by the ligand−protein and the ligand−heme interaction energies, the changes in conformational energies, the changes in solvation energies, and the entropic changes due to ligand binding. For an in-depth investigation of all of these factors, the dynamics and the electronic details of the systems should be taken into account at a high level of theory to accurately describe transition metal interactions. As this would be prohibitively computing intensive, we tried instead to deduce trends from static QM calculations and from classical MD simulations.

2.8. QM Calculations. To investigate the interaction energy between the ligands and the heme cofactor, we optimized the structures of the 36 azole compounds using DFT calculations. For all ligands with more than one local
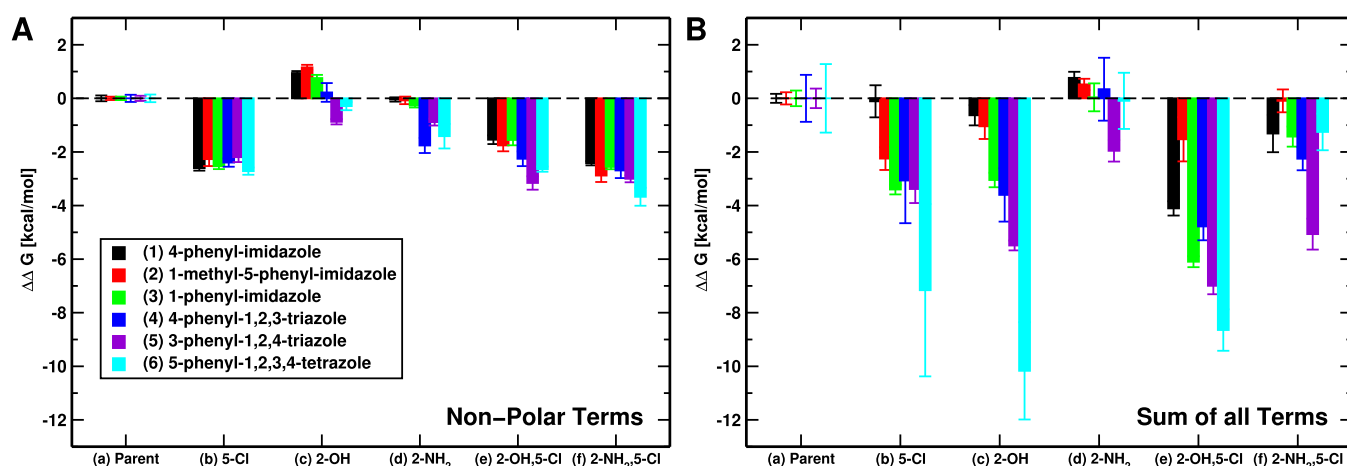
Figure 8. MM-GBSA calculations for azole compounds. (A) Non-polar contributions of substituted compounds relative to their parent compound. (B) Sum of all polar contributions of substituted compounds relative to their parent compound. Standard errors are indicated by error bars. The absolute values can be found in the Supporting Information, Figure S7.

energy minimum, we assumed the conformation where the *o*-hydroxy and *o*-amino groups could donate a hydrogen bond to Ser167 and the *m*-chloro substituent would be located in the identified hydrophobic subpocket (Supporting Information Figure S5). After careful investigation of many variables and different charge partitioning schemes, we chose to use the atomic Hirshfeld charge on the iron-binding nitrogen atom as a proxy for the basicity of the site and its heme binding strength because this was the only observable that correlated with known basicities of different scaffolds and that reproduced the ordering of the activities of the six parent compounds.

As shown in Figure 7A, there is a correlation between the charge on that atom and the activity of the compound. The more basic or electron-rich the nitrogen atom is, the higher the activity. The deprotonated 1,2,3-triazole **4a** has the most negative charge (−0.245), the tetrazole **6a** the least negative charge (−0.186), and the imidazoles display charges in between these values. For the 1,2,4-triazole **5a**, we calculated the charge both for the neutral (purple left triangle) and for the negatively charged (orange left triangle) compound. Interestingly, neither value obeys the correlation found for the other compounds, but the average of both values (black left triangle) provides the best correlation (correlation coefficient 0.862, standard deviation 0.69 kcal/mol). This shows that the deprotonated form of **5a** has a very high affinity for IDO1, but the neutral form is prevalent under experimental conditions. More sophisticated pK_a-based models may be used to estimate the ratio of deprotonated to neutral compound but are unlikely to yield additional insights. The activity of the 4-phenyl-imidazole **1a** is underestimated by the regression for an unknown reason.

Figure 7B shows the same data as part A but for the activities of the *m*-chloro-substituted compounds. A very similar correlation emerges between the different azole scaffolds, but all values are shifted toward a better activity, although the magnitude of charges decreases for each scaffold due to the electron-withdrawing substituent. This demonstrates that the *m*-chloro substituent increases activity mainly by interaction with the protein environment, as supported by the structural data. Again, the average charge of the 1,2,4-triazole **5b** fits well with the regression. For the compounds with *ortho* substituents, the correlation between atomic charge and compound activity becomes less clear (Supporting Information, Figure S6).

In order to better understand the effects of the *ortho* substituents, we optimized the structures of the azoles bound to a ferric iron−porphin−imidazole system as a model of the heme cofactor. Solvation effects were taken into account *via* a polarizable continuum model. We chose to use the ligand nitrogen to heme iron bond distance as a proxy for the binding strength because this avoids the use of an unbound ligand reference structure, which is challenging to unambiguously define. All optimized structures are shown in the Supporting Information Figure S7, and the calculated absolute bond lengths are shown in Figure S8.

Not surprisingly, the results of the calculations (Figure S7) show no correlation to the IDO1 inhibitory activities (Figure 2A) because all protein interactions are neglected. However, a few things can be deduced from the results. For all compounds, the 5-chloro substitution leads to a decrease in binding strength, while the 2-hydroxy substitution leads to an increase in binding strength (Figure 7C). Interestingly, the 2-amino substitution is favorable only for the 1,2,4-triazole and the tetrazole and unfavorable for all other scaffolds. This is probably related to the fact that only in the 1,2,4-triazole and the tetrazole, the 2-amino substituent can make a favorable electrostatic interaction with a nitrogen atom (leading to an essentially planar conformation), while in all other scaffolds, it is oriented toward a CH group, leading to a twisted conformation (Figure 7D), unfavorable in the protein environment.

2.9. Molecular Mechanics-Generalized Born Surface Area Calculations. Classical MD simulations suffer from shortcomings in the ligand force fields and in describing the electronic interactions with the heme cofactor, but they give insight into the dynamics of ligand−protein interactions. The molecular mechanics-Generalized Born surface area (MM-GBSA) is a popular method for free energy prediction, where the binding free energy ΔG_{bind} is decomposed into the sum of the gas-phase binding enthalpy, the desolvation free energy, and an entropic contribution.[84] The electrostatic part of the desolvation free energy is estimated using a Generalized Born (GB) model, while the non-polar part is assumed to be proportional to the solvent-accessible surface area. Because of
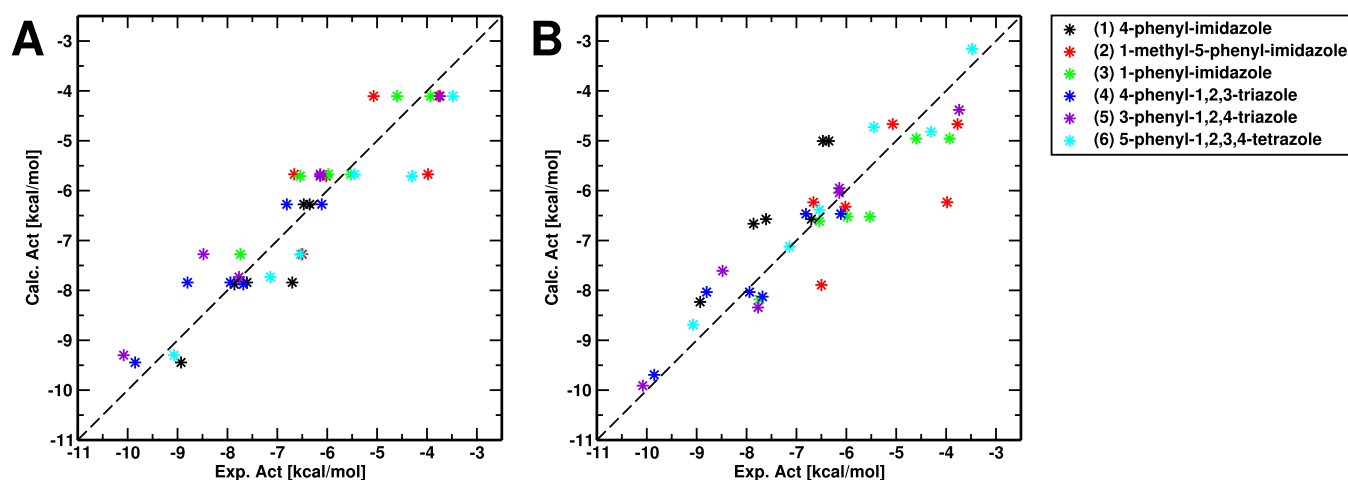
Figure 9. QSAR relationships. (A) Using four binary variables as descriptors (see text). (B) Using three binary variables and the charge density on the iron-binding nitrogen atom as descriptors.

its computational efficiency and accuracy, MM-GBSA has been widely used in biomolecular studies and in drug design.[85,86]

Here, we carried out MM-GBSA calculations for all compounds of Table 1. During the MD simulations, a covalent iron—ligand nitrogen bond was introduced, but for analysis, all ligand interactions with the heme porphyrin and His346 were excluded because they are badly described within the classical approach and introduce high fluctuations. The largest contributions to the binding free energies stem from residues Ala264, Ser167, Ser263, Tyr126, Gly262, and Val130 (Supporting Information, Figure S9C).

The electrostatic interactions favor the neutral ligands over the negatively charged ones (Figure S9A) and are slowly converging, especially for the charged ligands. The relative ordering of the binding free energies of the different azole scaffolds does not correlate with the experimental data as expected from the neglect of part of the interactions. We therefore display just the differences due to the phenyl substituents in Figure 8. It can be concluded from the results that (i) the 5-chloro substituent makes favorable interactions with the protein, mainly through non-polar (van der Waals) forces; (ii) the 2-hydroxy substituent makes favorable interactions with the protein, mainly through electrostatic interactions; and (iii) the 2-amino substituent is favorable for some compounds and detrimental for others. As expected, the 2-hydroxy and the 2-amino substituent mainly influence the interaction with Ser167 in the active site (Figure S9B).

2.10. Quantitative Structure—Activity Relationship and Application to Other Compounds. With the information gathered by classical and quantum chemical calculations, we developed a new quantitative structure—activity relationship (QSAR) model, as the one we previously developed for 1,2,3-triazoles[50] proved not to be transferable to other heterocycles. Despite many trials, QSAR models taking into account the MM-GBSA and DFT energies and combinations thereof did not display a good correlation with the experimentally measured values. However, a multiple linear regression on a simple binary matrix provided a correlation coefficient of 0.922 with a standard deviation of 0.706 kcal/mol (Figure 9A) and a correlation coefficient of 0.896 (standard deviation 0.812 kcal/mol) with the leave-one-out method. The four variables are (i) the presence of a m-chloro substituent, (ii) the presence of a o-hydroxy substituent, (iii)

the presence of a o-amino substituent making an intramolecular interaction with a nitrogen atom, and (iv) the presence of a 4-phenyl-imidazole or a 4-phenyl-1,2,3-triazole scaffold. The last variable captures the observed preference of hIDO1 to bind to these scaffolds, which can be explained by the basicity or negative charge density on the iron-binding nitrogen atom (Figure 7A). In fact, the fourth variable can be replaced by the Hirshfeld charge on the iron-binding nitrogen atom of the parent compound for each scaffold. This provides a correlation with a correlation coefficient of 0.893 (sd 0.821 kcal/mol) and a correlation coefficient of 0.865 (sd 0.917 kcal/mol) with the leave-one-out method (Figure 9B).

From the graphs, it is clear that the second model underestimates the 4-imidazole activities (black) and over-estimates the activities of the other imidazoles (green and red), which is probably due to steric factors unaccounted for in the model.

We applied this last model to other unsubstituted scaffolds of similar shape and type, compounds 7—35 shown in Figure 10. For each compound, we optimized the structure and calculated the Hirshfeld charge on the hypothetically iron-binding nitrogen atom, circled in blue. We tested compounds 7, 9, 15, 17, 20—23, and 29 in the enzymatic assay. In Figure 10, enzymatic activity is indicated by a green frame even if the IC$_{50}$ value is the millimolar range, inactivity by a red frame, and absence of experimental data by no frame (for details, see Table S3 in the Supporting Information). It is clear that the Hirshfeld charges, which are related to the basicity of the nitrogen atom, allow to distinguish between active and inactive scaffolds. With two exceptions (compounds 15 and 34), all compounds with a charge smaller than −0.18 are inactive. With one exception (compound 28), all compounds with a charge larger than −0.18 are active. This could indicate that sterically the benzo-compounds 26 to 29 are less favorable than the phenyl compounds because of suboptimal filling of pocket A. Scaffolds 30 and 31 have been used before in IDO1 inhibitors, and interestingly, a large increase in activity was observed when passing from scaffold 31 to 30, in agreement with the higher charge density on the nitrogen.[30−33,55] Interestingly, our results suggest testing compound 10, as it is predicted to be active on IDO1.
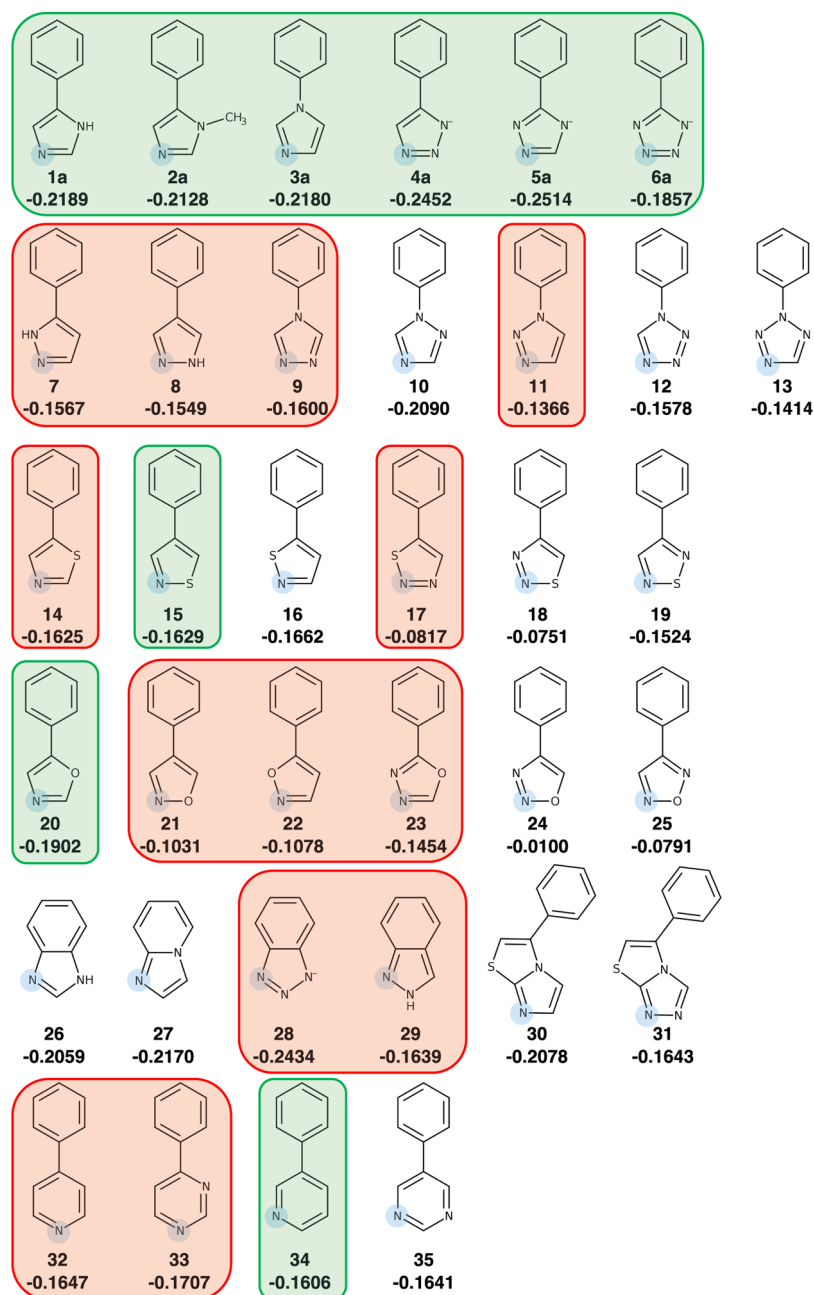
Figure 10. Other potential IDO1 inhibitor scaffolds. Hirshfeld charges on the nitrogen atom circled in blue are indicated. Inactive compounds are framed in red, active ones in green.

3. CONCLUSIONS

Despite the clinical failure of epacadostat, recent findings suggest that IDO1 is a player in many different pathways. Well-characterized and potent IDO1 inhibitors will be instrumental in deciphering its precise biological role. Here, we have presented experimental data for a set of closely related small heterocyclic compounds with more than 4 orders of magnitude differences in their IDO1 inhibitory activities ranging from millimolar to nanomolar levels. Based on structural data, classical MD simulations, and density functional theory calculations, we developed a model that rationalizes the observed activities and that can be applied to predict the activities of novel scaffolds. This may be important for expanding the currently very limited number of known high-affinity heme-binding IDO1 inhibitor scaffolds.

4. EXPERIMENTAL SECTION

4.1. Chemistry. *4.1.1. General Remarks.* All commercially available reagents and solvents (Fluka, Aldrich, Acros) were used without further purification. For reactions requiring anhydrous conditions, dry solvents were bought (Fluka, Aldrich). Reactions were monitored by TLC (Merck; silica gel 60 F254 plates) and detected with UV light, $KMnO_4$. Purifications were performed using flash chromatography (FC) on silica gel (SiO_2; Merck no. 9385 silica gel 60 Å, 230−400 mesh). IR Spectra: Perkin-Elmer Paragon 1000 FT-IR spectrometer. Mass spectra were recorded on a Nermag R 10−10C instrument in the chemical ionization mode. Electrospray mass analyses were recorded on a Finnigan MAT SSQ 710C spectrometer in the positive ionization mode. ^{1}H and ^{13}C NMR spectra were recorded on a Bruker-DPY-400 or a Bruker-ARX-400 spectrometer at 400 and 100.6 MHz, respectively. Data for ^{1}H NMR spectra are reported as follows: chemical shift, multiplicity, apparent coupling

constant, and integration. Data for ^{13}C NMR spectra are reported in terms of chemical shifts. Chemical shifts are given in parts per million, relative to an internal standard such as residual solvent signals. Coupling constants are given in hertz (Hz). High-resolution mass spectra were recorded via ESI−TOF−HRMS or MALDI−TOF−HRMS. The purity of all novel compounds was assessed by ^{1}H NMR and analytical HPLC (UV 220 nm) using a PFP propyl column (RESTEK Allure HPLC column, particle size 5 μm, pore size 60 Å, dimensions 150 × 4.6 mm) with a linear gradient of solvent B (acetonitrile, 0.1% TFA) over solvent A (H$_2$O, 0.1% TFA) from 0 to 100% in 30 min at a flow rate of 1 mL/min. Typically, 5 μL solution (0.5 mg/mL in 50% ACN/H$_2$O) was injected for each compound. The measured purity of all compounds was 95% or higher.

4.1.2. Procedures. 4.1.2.1. General Procedure for the Synthesis of Imidazole Derivatives (1b−1f).[20,59] A solution of α-bromoacetophenone derivatives (2 mmol, 1 equiv) was heated to 170−180 °C in formamide (12 mL) for 3−8 h. The solution was allowed to cool to room temperature (r.t) and the mixture was diluted with a saturated aq. soln. of NaHCO$_3$ (8 mL). The aqueous phase was extracted with EtOAc (3 × 10 mL). The combined organic extracts were washed successively with water and brine, then dried (Na$_2$SO$_4$), and concentrated in vacuo to afford a residue which was purified by flash column chromatography on silica gel to afford compounds 1b−1f.

4-(3-Chlorophenyl)-1H-imidazole (1b).[87] Synthesized from 2-bromo-(3-chlorophenyl)ethanone (36b) and formamide according to the general procedure to afford 1b as a white solid in 70% yield. ^{1}H NMR (400 MHz, CDCl$_3$): δ 7.78 (t, J = 1.9 Hz, 1H), 7.74 (s, 1H), 7.69−7.64 (m, 1H), 7.34 (t, J = 7.8 Hz, 1H), 7.25 (ddd, J = 8.0, 2.1, 1.1 Hz, 1H), ^{13}C NMR (100 MHz, CD$_3$OD): δ 137.65, 136.07, 135.32, 134.32, 129.81, 126.22, 124.30, 122.70, 115.19, ESI−TOF−HRMS m/z: calcd for (M + H) C$_9$H$_8$ClN$_2$, 179.0371; found, 179.0367.

2-(1H-Imidazole-4-yl)phenol (1c).[20] Synthesized from 2-(2-bromoacetyl)phenol (36c) and formamide according to the general procedure to afford 1c as a white solid in 60% yield. ^{1}H NMR (400 MHz, CD$_3$OD): δ 7.75 (d, J = 1.3 Hz, 1H), 7.63 (dd, J = 7.7, 1.7 Hz, 1H), 7.54 (d, J = 1.2 Hz, 1H), 7.13−7.04 (m, 1H), 6.90−6.80 (m, 2H), ^{13}C NMR (100 MHz, CD$_3$OD): δ 154.71, 133.64, 127.36, 125.13, 118.99, 117.80, 115.95, 114.02, ESI−TOF−HRMS m/z: calcd for (M + H) C$_9$H$_9$N$_2$O, 161.0709; found, 161.0705.

2-(1H-Imidazole-4-yl) aniline (1d).[59] Synthesized from 2-bromo-1-(2-nitrophenyl)ethan-1-one (37) and formamide according to the general procedure to afford 5-(2-nitrophenyl)-1H-imidazole. ^{1}H NMR (400 MHz, CD$_3$OD): δ 9.08 (d, J = 1.4 Hz, 1H), 8.29 (dd, J = 8.1, 1.4 Hz, 1H), 7.94−7.80 (m, 2H), 7.78 (d, J = 1.4 Hz, 1H), 7.74 (dd, J = 7.5, 1.6 Hz, 1H). 5-(2-Nitrophenyl)-1H-imidazole (1 equiv) was dissolved in methanol and treated with ferric chloride (0.33 equiv), activated carbon (1.70 equiv), and hydrazine hydrate (20 equiv). The resulting mixture was stirred at r.t. for 5 min and then heated to 70 °C for 48 h. The mixture was cooled to r.t and the solid was filtered off and washed with methanol. The liquids were combined and the solvent was removed under reduced pressure. The residue was purified by flash chromatography to afford 1d as a white solid in 25% yield for two steps. ^{1}H NMR (400 MHz, CD$_3$OD): δ 7.77 (s, 1H), 7.37 (dd, J = 7.7, 1.5 Hz, 1H), 7.31 (s, 1H), 7.10−7.03 (m, 1H), 6.83 (d, J = 8.0 Hz, 1H), 6.74 (t, J = 7.5 Hz, 1H). ^{13}C NMR (100 MHz, CD$_3$OD): δ 148.06, 134.49, 133.77, 133.00, 131.54, 129.45, 125.15, 121.27, 117.80; ESI−TOF−HRMS m/z: calcd for (M + H) C$_9$H$_9$ClN$_3$, 160.0867; found, 160.0866.

4-Chloro-2-(1H-imidazole-4-yl)phenol (1e).[21] Synthesized from 4-chloro-2-(2-bromoacetyl) phenol (36e) and formamide according to the general procedure to afford 1e as a light yellow solid in 75% yield. ^{1}H NMR (400 MHz, CDCl$_3$): δ 12.23 (br s, −OH, 1H), 9.39 (br s, −OH, 1H), 7.77 (d, J = 1.2 Hz, 1H), 7.45 (d, J = 2.6 Hz, 1H), 7.39 (d, J = 1.2 Hz, 1H), 7.12 (dd, J = 8.7, 2.6 Hz, 1H), 6.94 (d, J = 8.8 Hz, 1H), ^{13}C NMR (100 MHz, CD$_3$OD): δ 153.57, 136.86, 133.95, 126.78, 124.58, 123.61, 119.65, 117.33, 114.43, ESI−TOF−HRMS m/z: calcd for (M + H) C$_9$H$_8$ClN$_2$O, 195.0320; found, 195.0316.

4-Chloro-2-(1H-imidazole-4-yl)aniline (1f). Synthesized from 2-bromo-1-(5-chloro-2-nitrophenyl)ethan-1-one[88] (38) and formamide according to the general procedure to afford 5-(5-chloro-2-nitrophenyl)-1H-imidazole. ^{1}H NMR (400 MHz, CD$_3$OD): δ 9.09 (d, J = 1.4 Hz, 1H), 8.31 (d, J = 8.8 Hz, 1H), 7.90−7.80 (m, 3H). 5-(5-Chloro-2-nitrophenyl)-1H-imidazole (1 equiv) was dissolved in methanol and treated with ferric chloride (0.33 equiv), activated carbon (1.70 equiv), and hydrazine hydrate (20 equiv). The resulting mixture was stirred at r.t. for 5 min and then heated to 70 °C for 48 h. The mixture was cooled to r.t. and the solid was filtered off and washed with methanol. The liquids were combined and the solvent was removed under reduced pressure. The residue was purified by flash chromatography to afford 1f as a white solid in 30% yield (over two steps). ^{1}H NMR (400 MHz, CD$_3$OD): δ 7.83 (d, J = 2.3 Hz, 1H), 7.80−7.76 (m, 2H), 7.50 (dd, J = 8.6, 2.3 Hz, 1H), 7.37 (d, J = 1.1 Hz, 1H), ^{13}C NMR (100 MHz, CD$_3$OD): δ 146.39, 139.66, 134.80, 132.75, 131.32, 128.34, 126.93, 123.30, 118.39; ESI−TOF−HRMS m/z: calcd for (M + H) C$_9$H$_{10}$N$_3$, 194.0480; found, 194.0476.

4.1.2.2. General Procedure for the C5 Arylation of N-Methylimidazoles (2a−f).[59−61] The aryl iodide (1 mmol, 1 equiv) was combined with 1-methyl-1H-imidazole (4 mmol, 4 equiv), Pd (OAc)$_2$ (5 mol %, 0.05 equiv), tricyclohexylphosphonium tetrafluoroborate (10 mol %, 0.1 equiv), and Cs$_2$CO$_3$ (1 mmol, 1 equiv) in DMF (4 mL). The mixture was heated to 120 °C for 15 h. After cooling to r.t., the solids were filtered off and the solution was partitioned between EtOAc and H$_2$O. The organic layer was collected, and the H$_2$O layer was extracted with EtOAc (2 × 5 mL). The combined extracts were washed with a saturated aq. soln. of NaHCO$_3$ and dried over Na$_2$SO$_4$. The solvent was removed under vacuum and the residue was purified by column chromatography on silica gel to afford 2a−2f.

1-Methyl-5-phenyl-1H-imidazole (2a).[89] Synthesized from 1-iodobenzene (39a) and N-methylimidazole according to the general procedure to afford 2a as a white solid in 35% yield. ^{1}H NMR (400 MHz, CDCl$_3$): δ 7.59 (s, 1H), 7.51−7.36 (m, 5H), 7.17 (s, 1H), 3.70 (s, 3H). ^{13}C NMR (100 MHz, CD$_3$COCD$_3$): δ 139.65, 130.42, 128.70, 128.08, 127.76, 127.48, 31.92; ESI−TOF−HRMS m/z: calcd for (M + H) C$_{10}$H$_{11}$N$_2$, 159.0917; found, 159.0913.

1-Methyl-5-(3-chlorophenyl)-1H-imidazole (2b). Synthesized from 1-chloro-3-iodobenzene (39b) and N-methylimidazole according to the general procedure to afford 2b as an oil in 60% yield. ^{1}H NMR (400 MHz, CDCl$_3$): δ 7.52 (s, 1H), 7.39−7.26 (m, 3H), 7.25 (dt, J = 7.2, 1.7 Hz, 1H), 7.10 (s, 1H), 3.66 (s, 3H); ^{13}C NMR (100 MHz, CDCl$_3$): δ 139.51, 134.59, 132.06, 131.51, 130.03, 128.55, 128.25, 127.94, 126.45, 32.65, ESI−TOF−HRMS m/z: calcd for (M + H) C$_{10}$H$_{10}$ClN$_2$, 193.0527; found, 193.0524.

2-(1-Methyl-1H-imidazole-5-yl)phenol (2c, CAS 1781522-02-8). Synthesized from 2-iodoanisole (40) and N-methylimidazole according to the general procedure to afford crude 2-(1-methyl-1H-imidazole-5-yl)anisole. ^{1}H NMR (400 MHz, CD$_3$OD): δ 7.73 (s, 1H), 7.46 (ddd, J = 8.3, 7.4, 1.8 Hz, 1H), 7.26 (dd, J = 7.5, 1.8 Hz, 1H), 7.13 (dd, J = 8.4, 1.1 Hz, 1H), 7.05 (td, J = 7.5, 1.1 Hz, 1H), 6.92 (s, 1H), 3.85 (s, 3H), 3.55 (s, 3H). 2-(1-Methyl-1H-imidazole-5-yl)anisole (1.0 mmol) was dissolved in 48% hydrobromic acid (HBr) in water (4 mL) and the orange solution was heated to 100 °C for 14 h under N$_2$. The solution was cooled to r.t., diluted with water, and neutralized by the addition of a saturated aq. soln. of NaHCO$_3$ until the evolution of CO$_2$ ceased. The organic product was extracted with ethyl acetate. The extract was dried over sodium sulfate and concentrated in vacuo to afford a residue that was purified by flash column chromatography on silica gel to afford 2c as a white solid in 60% yield (over two steps). ^{1}H NMR (400 MHz, CD$_3$OD): δ 7.78 (s, 1H), 7.29 (ddd, J = 8.2, 7.4, 1.7 Hz, 1H), 7.20 (dd, J = 7.5, 1.7 Hz, 1H), 6.97−6.86 (m, 3H), 3.62 (s, 3H), ^{13}C NMR (100 MHz, CD$_3$OD): δ 155.44, 131.71, 130.03, 126.38, 119.29, 116.44, 115.27, 31.13, ESI−TOF−HRMS m/z: calcd for (M + H) C$_{10}$H$_{11}$N$_2$O, 175.0866; found, 175.0862.

2-(1-Methyl-1H-imidazole-5-yl)aniline (2d, CAS 1780550-29-9). Synthesized from 2-iodonitrobenzene (42) and N-methylimidazole according to the general procedure to afford 1-methyl-5-(2-nitro-

phenyl)-1H-imidazole. ^{1}H NMR (400 MHz, CDCl$_3$): δ 8.04−7.90 (m, 2H), 7.66−7.60 (m, 2H), 7.58−7.50 (m, 1H), 7.39 (dd, J = 7.5, 1.6 Hz, 1H), 3.42 (s, 3H). 1-Methyl-5-(2-nitrophenyl)-1H-imidazole (1 equiv) was dissolved in methanol and treated with ferric chloride (0.33 equiv), activated carbon (1.70 equiv), and hydrazine hydrate (20 equiv). The resulting mixture was stirred at r.t. for 5 min before heating to 70 °C for 48 h. The mixture was cooled to r.t., and then the solid was filtered off and washed with methanol. The liquids were combined, and the solvent was removed under reduced pressure. The residue was purified by flash chromatography to afford **2d** as a brown solid in 60% yield (over two steps). ^{1}H NMR (400 MHz, CD$_3$OD): δ 7.65 (s, 1H), 7.06 (ddd, J = 8.1, 7.3, 1.6 Hz, 1H), 6.90 (dd, J = 7.6, 1.6 Hz, 1H), 6.84 (s, 1H), 6.71 (dd, J = 8.2, 1.2 Hz, 1H), 6.61 (td, J = 7.4, 1.2 Hz, 1H), 3.41 (s, 3H); ^{13}C NMR (100 MHz, CD$_3$OD): δ 146.86, 138.35, 131.30, 130.79, 129.91, 126.25, 117.17, 115.25, 113.67, 30.84; ESI−TOF−HRMS m/z: calcd for (M + H) C$_{10}$H$_{11}$N$_3$, 174.1029; found, 174.1040.

4-Chloro-2-(1-methyl-1H-imidazol-5-yl)phenol (**2e**, CAS 2107720-24-9). Synthesized from 2-iodo-4-chloroanisole (**41**) and N-methylimidazole according to the general procedure to afford the crude 4-chloro-2-(1-methyl-1H-imidazol-5-yl)anisole. ^{1}H NMR (400 MHz, CD$_3$OD): δ 7.71 (s, 1H), 7.45 (dd, J = 8.8, 2.7 Hz, 1H), 7.27 (d, J = 2.7 Hz, 1H), 7.13 (d, J = 8.9 Hz, 1H), 6.94 (s, 1H), 3.85 (s, 3H), 3.56 (s, 3H). 4-Chloro-2-(1-methyl-1H-imidazol-5-yl)anisole (1.0 mmol) was dissolved in 48% HBr in water (4 mL) and the orange solution was heated to 100 °C for 14 h under N$_2$. The mixture was cooled to r.t., diluted with water, and neutralized by the addition of a saturated aq. soln. of NaHCO$_3$ until the evolution of CO$_2$ ceased. The organic layer was extracted with ethyl acetate (2 × 5 mL), dried over sodium sulfate, and concentrated in vacuo to afford a residue that was purified by flash column chromatography on silica gel to afford **2e** as a white solid in 70% yield for two steps. ^{1}H NMR (400 MHz, CD$_3$OD): δ 7.58 (s, 1H), 7.15 (dd, J = 8.7, 2.7 Hz, 1H), 7.08 (d, J = 2.7 Hz, 1H), 6.83 (s, 1H), 6.79 (d, J = 8.7 Hz, 1H), 3.50 (s, 3H); ^{13}C NMR (100 MHz, CD$_3$OD): δ 154.37, 138.41, 131.01, 130.05, 129.67, 126.91, 123.68, 118.23, 116.70, 31.23; ESI−TOF−HRMS m/z: calcd for (M + H) C$_{10}$H$_{10}$ClN$_2$O, 209.0476; found, 209.0472.

4-Chloro-2-(1-methyl-1H-imidazol-5-yl)aniline (**2f**, CAS 2106580-97-4). Synthesized from 2-iodo-4-chloronitrobenzene (**43**) and N-methylimidazole according to the general procedure to afford 5-(5-chloro-2-nitrophenyl)-1-methyl-1H-imidazole. ^{1}H NMR (400 MHz, CDCl$_3$): δ 8.75 (s, 1H), 8.12 (d, J = 8.8 Hz, 1H), 7.64 (dd, J = 8.8, 2.2 Hz, 1H), 7.47 (d, J = 2.3 Hz, 1H), 7.18 (s, 1H), 3.61 (s, 3H). 5-(5-Chloro-2-nitrophenyl)-1-methyl-1H-imidazole (1 equiv) was dissolved in methanol and treated with ferric chloride (0.33 equiv), activated carbon (1.70 equiv), and hydrazine hydrate (20 equiv). The resulting mixture was stirred at r.t. for 5 min before heating to 70 °C for 48 h. The mixture was cooled to r.t., and then the solid was filtered off and washed with methanol. The liquids were combined, and the solvent was removed under reduced pressure. The residue was purified by flash chromatography to afford **2f** as a white solid in 65% yield for two steps. ^{1}H NMR (400 MHz, CD$_3$OD): δ 7.75 (s, 1H), 7.16 (dd, J = 8.7, 2.5 Hz, 1H), 7.04 (d, J = 2.5 Hz, 1H), 6.98 (s, 1H), 6.81 (d, J = 8.7 Hz, 1H), 3.56 (s, 3H); ^{13}C NMR (100 MHz, CD$_3$OD): δ 145.96, 138.82, 130.58, 129.59, 126.99, 121.11, 116.29, 115.04, 30.80; ESI−TOF−HRMS m/z: calcd for (M + H) C$_{10}$H$_{11}$ClN$_3$, 208.0641; found, 208.0643.

4.1.2.3. General Procedure for the Synthesis of N-Phenylimidazole Derivatives (3c, 3e, and 3f).[61,62] The aryl iodide (1 mmol, 1 equiv) was dissolved in DMF and treated with N,N-dimethylethane-1,2-diamine (0.3 mmol, 0.3 equiv), Cs$_2$CO$_3$ (2 mmol, 2.0 equiv), CuI (0.1 mmol, 0.1 equiv), and 1H-imidazole (2.0 mmol, 2.0 equiv) under an N$_2$ atmosphere. The mixture was stirred at 140 °C for 12 h. After cooling to r.t., the solids were filtered off and washed with dichloromethane (2 × 5 mL). The combined organic phases were concentrated under reduced pressure and the residue was purified by flash column chromatography on silica gel to afford **3c**, **3e**, and **3f**.

2-(1H-Imidazol-1-yl)phenol (**3c**).[90] Synthesized from 1-iodoanisole (**40**) and 1H-imidazole according to the general procedure to

afford 2-(1H-imidazol-1-yl)anisole. ^{1}H NMR (400 MHz, CD$_3$OD): δ 7.97 (s, 1H), 7.51−7.37 (m, 3H), 7.24 (d, J = 8.9 Hz, 1H), 7.13 (s, 1H), 6.96 (m, 1H), 3.90 (s, 3H). 2-(1H-Imidazol-1-yl)anisole was dissolved in 48% HBr in water (4 mL) and the orange solution was heated to 100 °C for 14 h under N$_2$. The mixture was cooled to r.t., then diluted with water, and neutralized by the addition of a saturated aq. soln. of NaHCO$_3$ until the evolution of CO$_2$ ceased. The mixture was extracted with ethyl acetate (2 × 5 mL), and the combined extracts were dried over sodium sulfate and concentrated in vacuo to afford a residue that was purified by flash column chromatography on silica gel to afford **3c** as a white solid in 65% yield (over two steps). ^{1}H NMR (400 MHz, CD$_3$OD): δ 7.96 (d, J = 1.2 Hz, 1H), 7.40 (t, J = 1.4 Hz, 1H), 7.33 (dd, J = 7.9, 1.6 Hz, 1H), 7.26 (ddd, J = 8.2, 7.4, 1.6 Hz, 1H), 7.11 (s, 1H), 7.04 (dd, J = 8.2, 1.3 Hz, 1H), 6.97 (td, J = 7.7, 1.4 Hz, 1H), ^{13}C NMR (100 MHz, CD$_3$OD): δ 150.54, 128.73, 127.04, 125.03, 124.73, 120.36, 119.66, 116.50, ESI−TOF−HRMS m/z: calcd for (M + H) C$_9$H$_9$N$_2$O, 161.0709; found, 161.0706.

4-Chloro-2-(1H-imidazol-1-yl)phenol (**3e**).[91] Synthesized from 4-chloro-2-iodoanisole (**41**) and 1H-imidazole according to the general procedure to afford 4-chloro-2-(1H-imidazol-1-yl)anisole. ^{1}H NMR (400 MHz, CDCl$_3$): δ 7.82 (d, J = 1.1 Hz, 1H), 7.38−7.29 (m, 2H), 7.25−7.14 (m, 2H), 7.01 (d, J = 8.8 Hz, 1H), 3.87 (s, 3H). 4-Chloro-2-(1H-imidazol-1-yl)anisole was dissolved in 48% HBr in water (4 mL) and the orange solution was heated to 100 °C for 14 h under N$_2$. The mixture was cooled to r.t, then diluted with water, and neutralized by the addition of a saturated aq. soln. of NaHCO$_3$ until the evolution of CO$_2$ ceased. The mixture was extracted with ethyl acetate. The combined extracts were dried over Na$_2$SO$_4$ and concentrated in vacuo to afford a residue that was purified by flash column chromatography on silica gel to afford **3e** as a white solid in 52% yield (over two steps). ^{1}H NMR (400 MHz, CD$_3$OD): δ 8.04 (s, 1H), 7.46 (s, 1H), 7.42 (d, J = 2.5 Hz, 1H), 7.27 (dd, J = 8.7, 2.6 Hz, 1H), 7.14 (s, 1H), 7.02 (d, J = 8.8 Hz, 1H), ^{13}C NMR (100 MHz, CD$_3$OD): δ 149.43, 128.47, 125.53, 124.77, 123.96, 117.69, ESI−TOF−HRMS m/z: calcd for (M + H) C$_9$H$_8$ClN$_2$O, 195.0320; found, 195.0315.

2-(1H-Imidazol-1-yl)aniline (**3f**, CAS 190200-15-8). Synthesized from 4-chloro-2-iodoaniline (**39f**) and 1H-imidazole according to the general procedure to afford **3f** as a white solid in 75% yield. ^{1}H NMR (400 MHz, CD$_3$OD): δ 7.82 (s, 1H), 7.30 (s, 1H), 7.21 (dd, J = 8.8, 2.4 Hz, 2H), 7.16 (d, J = 2.4 Hz, 1H), 6.90 (d, J = 8.7 Hz, 1H), ^{13}C NMR (100 MHz, CD$_3$OD): δ 142.27, 137.56, 129.37, 128.40, 126.38, 123.16, 121.06, 120.43, 117.28, ESI−TOF−HRMS m/z: calcd for (M + H) C$_9$H$_9$ClN$_3$, 194.0480; found, 194.0476.

4.1.2.4. General Procedure for the Synthesis of 1,2,4-Triazoles (5b−c and 5e−g).[63] A solution of amide (**44b−c**, **44e−g**) (1.0 mmol, 1 equiv) and N,N-dimethylformamide−dimethyl acetal (DMF−DMA) (1.5 mL) was heated under reflux for 1 h under N$_2$. The mixture was concentrated under reduced pressure and the residue was washed with hexane. After drying in vacuo, a white solid was obtained that was used without purification in the next step. The crude product was dissolved in acetic acid (2 mL), and then hydrazine hydrate (1.1 mmol, 1.1 equiv) was added dropwise to the stirred solution. The mixture was stirred at 90 °C for 2 h. After cooling to r.t., the solvent was removed in vacuo. The mixture was taken with diethyl ether (5 mL) and stirred at 0 °C for 30 min. The precipitate was collected, dried under reduced pressure, and purified by flash column chromatography on silica gel to afford the corresponding triazoles (**5b−c**, **5e−g**).

3-(3-Chlorophenyl)-1H-1,2,4-triazole (**5b**).[92] Synthesized from 2-chlorobenzamide (**44b**) and hydrazine hydrate according to the general procedure to afford **5b** as a white solid in 50% yield. ^{1}H NMR (400 MHz, CDCl$_3$): δ 8.24 (s, 1H), 8.09 (q, J = 1.3 Hz, 1H), 7.97 (td, J = 4.4, 1.6 Hz, 1H), 7.43−7.40 (m, 2H). ^{13}C NMR (100 MHz, CD$_3$OD): δ 134.49, 130.12, 129.24, 125.92, 124.28; ESI−TOF−HRMS m/z: calcd for (M + H) C$_8$H$_7$ClN$_3$, 180.0323; found, 180.0319.

2-(1H-1,2,4-Triazol-3-yl)phenol (**5c**).[93] Synthesized from 2-hydroxybenzamide (**44c**) and hydrazine hydrate according to the general procedure to afford **5c** as a white fluffy powder in 75% yield.

O

^{1}H NMR (400 MHz, CD$_3$OD): δ 8.34 (s, 1H), 7.97 (dd, J = 7.8, 1.7 Hz, 1H), 7.34 (ddd, J = 8.7, 7.3, 1.7 Hz, 1H), 7.04–6.93 (m, 2H), ^{13}C NMR (100 MHz, CD$_3$OD): δ 156.33, 131.15, 126.60, 119.25, 116.47, 112.72, ESI–TOF–HRMS m/z: calcd for (M + H) C$_8$H$_8$N$_3$O, 162.0662; found, 162.0658.

4-Chloro-2-(1H-1,2,4-triazol-3-yl)phenol (5e, CAS 814263-35-9). Synthesized from 5-chloro-2-hydroxybenzamide (44e) and formic acid according to the general procedure to afford 5e as a white solid in 76% yield. ^{1}H NMR (400 MHz, CD$_3$OD): δ 8.44 (s, 1H), 7.99 (d, J = 2.6 Hz, 1H), 7.31 (dd, J = 8.8, 2.6 Hz, 1H), 6.99 (d, J = 8.8 Hz, 1H), ^{13}C NMR (100 MHz, CD$_3$OD): δ 155.10, 130.65, 125.97, 123.92, 118.28, 114.68, ESI–TOF–HRMS m/z: calcd for (M + H) C$_8$H$_7$ClN$_3$O, 196.0272; found, 196.0267.

4-Chloro-2-(1H-1,2,4-triazol-3-yl)aniline (5f, CAS 55138-98-2). Synthesized from 2-amino-5-chlorobenzamide (44f) and formic acid according to the general procedure to afford 5f as a white solid in 52% yield. ^{1}H NMR (400 MHz, CD$_3$COCD$_3$): δ 7.81 (s, 1H), 7.57 (d, J = 2.5 Hz, 1H), 7.10 (dd, J = 8.7, 2.5 Hz, 1H), 6.74 (d, J = 8.6 Hz, 1H), 6.39 (s, 1H); ^{13}C NMR (100 MHz, CD$_3$COCD$_3$): δ 151.43, 147.31, 141.10, 131.16, 123.33, 122.87, 116.63, 112.29; ESI–TOF–HRMS m/z: calcd for (M + H) C$_8$H$_8$ClN$_4$, 195.0437; found, 195.0441.

4-Bromo-2-(1H-1,2,4-triazol-3-yl)aniline (5g).[94] Synthesized from 2-amino-5-bromobenzamide (44g) and hydrazine hydrate according to the general procedure to afford 5g as a white solid in 35% yield. ^{1}H NMR (400 MHz, CD$_3$OD): δ 8.50 (s, 1H), 8.04 (s, 1H), 7.24 (dd, J = 8.8, 2.4 Hz, 1H), 6.78 (d, J = 8.7 Hz, 1H); ^{13}C NMR (100 MHz, CD$_3$OD): δ 145.55, 142.70, 132.04, 130.07, 117.80, 107.17; ESI–TOF–HRMS m/z: calcd for (M + H) C$_8$H$_8$BrN$_4$, 238.9927; found, 238.9922.

4.1.2.5. General Procedure for the Synthesis of 1,2,3,4-Tetrazoles (6c, 6e, and 6f).[64] A mixture of the corresponding carbonitrile (45c,e,f) (1 mmol, 1 equiv), NaN$_3$ (2 mmol, 3 equiv), and Et$_3$N·HCl (3.7 mmol, 3.7 equiv) in toluene (3 mL) was stirred at 99 °C overnight. After cooling to r.t., the mixture was extracted with H$_2$O (2 mL) and the aqueous phase was acidified by dropwise addition of conc. HCl affording a precipitate. The precipitate was collected, washed with H$_2$O (2 × 5 mL), dried under reduced pressure, and purified by flash column chromatography on silica gel to afford the corresponding products 6c, 6e, and 6f.

2-(1H-Tetrazol-5-yl)phenol (6c).[64] Synthesized from 2-hydroxybenzonitrile (45c) and NaN$_3$ according to the general procedure to afford 6c as a white solid in 80% yield. ^{1}H NMR (400 MHz, CD$_3$OD): δ 8.08 (dd, J = 7.8, 1.7 Hz, 1H), 7.44 (ddd, J = 8.3, 7.3, 1.7 Hz, 1H), 7.10–7.02 (m, 2H), ^{13}C NMR (100 MHz, CD$_3$OD): δ 155.63, 152.42, 132.74, 128.51, 119.80, 116.00, 109.76, ESI–TOF–HRMS m/z: calcd for (M + H) C$_7$H$_7$N$_4$O, 163.0614; found, 163.0612.

4-Chloro-2-(1H-tetrazol-5-yl)phenol (6e).[95] Synthesized from 5-chloro-2-hydroxybenzonitrile (45e) and NaN$_3$ according to the general procedure to afford 6d as a white solid in 70% yield. ^{1}H NMR (400 MHz, CD$_3$OD): δ 8.08 (d, J = 2.7 Hz, 1H), 7.42 (dd, J = 8.8, 2.7 Hz, 1H), 7.07 (d, J = 8.9 Hz, 1H); ^{13}C NMR (100 MHz, CD$_3$OD): δ 155.23, 152.78, 133.16, 128.69, 125.27, 118.99, 112.15; ESI–TOF–HRMS m/z: calcd for (M + H) C$_7$H$_6$ClN$_4$O, 197.0225; found, 197.0221.

4-Chloro-2-(1H-tetrazol-5-yl)aniline (6f).[96] Synthesized from 2-amino-5-chlorobenzonitrile (45f) and NaN$_3$ according to the general procedure to afford 6f as a white solid in 69% yield. ^{1}H NMR (400 MHz, CDCl$_3$): δ 7.71 (d, J = 2.5 Hz, 1H), 7.21 (dd, J = 8.8, 2.4 Hz, 1H), 6.78 (d, J = 8.8 Hz, 1H), ^{13}C NMR (100 MHz, CD$_3$OD): δ 155.11, 146.09, 131.40, 126.70, 120.42, 117.94, 106.45, ESI–TOF–HRMS m/z: calcd for (M + H) C$_7$H$_7$ClN$_5$, 196.0384; found, 196.0381.

4-Phenyl-4H-1,2,4-triazole (9).[65] To a solution of Cu(OAc)$_2$·H$_2$O (0.01 mmol, 0.01 equiv) in DMF (2 mL) were added phenyl iodide (1.2 mmol, 1.2 equiv), 4H-1,2,4-triazole (1.0 mmol, 1.0 equiv), and Cs$_2$CO$_3$ (2.0 mmol, 2.0 equiv) under a nitrogen atmosphere. The mixture was stirred at 110 °C for 24 h. After cooling to r.t., the mixture was partitioned between water and ethyl acetate. The organic layer was separated, and the aqueous layer was extracted with ethyl

acetate. The combined organic layers were washed with brine, dried over Na$_2$SO$_4$, and concentrated in vacuo. The residue was purified by flash chromatography on silica gel to afford 4-phenyl-4H-1,2,4-triazole (9) as a semi solid in 45% yield. ^{1}H NMR (400 MHz, CDCl$_3$): δ 8.59 (s, 1H), 8.14 (s, 1H), 7.75–7.67 (m, 2H), 7.59–7.50 (m, 2H), 7.48–7.39 (m, 1H), ^{13}C NMR (101 MHz, CDCl$_3$): δ 152.60, 140.87, 137.01, 129.80, 128.26, 120.10, ESI–TOF–HRMS m/z: calcd for (M + H) C$_8$H$_8$N$_3$, 146.0713; found, 146.0710.

4-Phenylisothiazole (15).[66] DMF (2.0 mL) was added dropwise to POCl$_3$ (9.0 mmol, 3.0 equiv) and cooled to 0 °C. Phenyl acetic acid (3.0 mmol, 1.0 equiv) was then added and the mixture was stirred at 85 °C for 2 h. The reaction mixture was cooled to room temperature and cracked ice was added to adjust the volume to ca. 15 mL. The reaction mixture was extracted with dichloromethane, the combined extracts were dried, and the solvents were evaporated to yield crude 2-phenyl-3-N,N-dimethylaminoacrolein as a yellow oil. NaOH (25% aq. soln., 6 mL) was added to crude 2-phenyl-3-N,N-dimethylaminoacrolein in EtOH (5.0 mL), and the reaction mixture was refluxed under stirring for 1 h. Ethanol was removed under vacuum, and the residue was diluted by addition of crushed ice and acidified (pH < 3) using aqueous HCl (1:1). The resulting mixtures were extracted with diethyl ether, the combined extracts were dried, and the solvents were evaporated to leave crude enolized 2-aryl malondialdehyde as a yellow oil. SOCl$_2$ (4.2 mL, 57.6 mmol) was added to crude 2-aryl malondialdehyde in CH$_2$Cl$_2$ (6 mL) and cooled to 0 °C, and the reaction mixtures were stirred at 0 °C for 1 h. The solvents were evaporated, and the crude product was used without purification in the next step. NH$_4$SCN (7.2 mmol, 4.0 equiv) was added to a solution of chloroacrolein (1.8 mmol, 1.0 equiv) in DMF (3.0 mL), and the reaction mixture was heated for 16 h at 70 °C under stirring. The reaction mixture was diluted with brine (20 mL) and extracted with ethyl acetate. The combined extract was dried, the solvent evaporated, and the residue was subjected to flash chromatography on silica gel to afford compound 15 as a white solid in 70% yield. ^{1}H NMR (400 MHz, CDCl$_3$): δ 8.81 (s, 1H), 8.74 (s, 1H), 7.66–7.59 (m, 2H), 7.51–7.45 (m, 2H), 7.48–7.34 (m, 1H), ^{13}C NMR (100 MHz, CDCl$_3$): δ 156.05, 142.69, 139.98, 132.59, 129.17, 128.07, 126.93, ESI–TOF–HRMS m/z: calcd for (M + H) C$_9$H$_8$NS, 162.0372; found, 162.0373.

5-Phenyl-1,2,3-thiadiazole (17).[67] To a solution of TMSCHN$_2$ (2 M ether solution, 0.6 mL, 1.2 mmol, 1.2 equiv) in diethylether (8 mL), n-BuLi (2.5 M hexane solution, 0.48 mL, 1.2 mmol, 1.2 equiv) was added dropwise at −78 °C under nitrogen, and the mixture was stirred at −78 °C for 20 min. A solution of methyl thiobenzoate (1.0 mmol, 1.0 equiv) in diethyl ether (3 mL) was then added dropwise at −78 °C. The mixture was stirred at −78 °C for 30 min and then at 0 °C for 30 min. After addition of water (1 mL) and methanol (5 mL), the mixture was stirred at r.t. for 1 h and concentrated in vacuo. The residue was suspended in water and extracted with ethyl acetate. The organic extracts were washed with water, saturated aq. NaCl, dried over anhydrous Na$_2$SO$_4$, and concentrated in vacuo. The residue was purified by column chromatography to afford 5-phenyl-1,2,3-thiadiazole (17) as a semi solid in 75% yield. ^{1}H NMR (400 MHz, CDCl$_3$): δ 8.90 (s, 1H), 7.67-7.61 (m, 2H), 7.57–7.47 (m, 3H), ^{13}C NMR (100 MHz, CDCl$_3$): δ 157.06, 144.18, 130.55, 129.60, 128.19, 127.45, ESI–TOF–HRMS m/z: calcd for (M + H) C$_8$H$_7$N$_2$S, 163.0324; found, 163.0323.

5-Phenyloxazole (20).[68] To a solution of benzaldehyde (1.0 mmol, 1.0 equiv) in MeOH (5 mL) was added K$_2$CO$_3$ (1.5 mmol, 1.5 equiv) and toluenesulfonylmethyl isocyanide (TosMIC, 1.0 mmol, 1.0 equiv). The reaction mixture was stirred for 2 h at 80 °C, cooled down to r.t., quenched with H$_2$O, and diluted with EtOAc. After removal of the organic layer, the aqueous layer was extracted with EtOAc. The organic layer was combined, dried over Na$_2$SO$_4$, filtered, and concentrated in vacuo. Flash chromatography afforded 5-phenyloxazole (20) as a white solid in 60% yield. ^{1}H NMR (400 MHz, CDCl$_3$): δ 7.95 (s, 1H), 7.72–7.65 (m, 2H), 7.50–7.42 (m, 2H), 7.39 (s, 2H), ^{13}C NMR (101 MHz, CD$_3$OD): δ 154.02, 147.65, 128.79, 128.61, 127.59, 126.00, 121.41, 121.39, ESI–TOF–HRMS m/z: calcd for (M + H) C$_9$H$_8$NO, 146.0600; found, 146.0599.

4-Phenylisoxazole (**21**).[69] To a solution of 2-phenylmalonaldehyde (1.0 mmol, 1.0 equiv) in EtOH (5 mL) was added hydroxylamine hydrochloride (2.0 mmol, 2.0 equiv). The reaction mixture was stirred for 2 h at 80 °C. After completion of the reaction, the solvents were removed under reduced pressure, and the crude product was dissolved in CH_2Cl_2 (2 × 5 mL) and washed with water (10 mL). The organic layers were combined, dried over Na_2SO_4, filtered, and concentrated *in vacuo*. Purification was accomplished by column chromatography on silica gel to afford compound **21** as a white solid in 80% yield. ^{1}H NMR (400 MHz, $CDCl_3$): δ 8.70 (s, 1H), 8.59 (s, 1H), 7.55−7.41 (m, 2H), 7.41−7.33 (m, 2H), 3.47 (s, 1H), ^{13}C NMR (100 MHz, $CDCl_3$): δ 153.38, 147.99, 129.21, 128.54, 128.12, 126.45, 121.41, ESI−TOF−HRMS *m/z*: calcd for (M + H) C_9H_8NO, 146.0600; found, 146.0597.

5-Phenyl-1,2,3-oxadiazole (**23**).[94] To a solution of benzoic hydrazide (2.0 mmol, 1 equiv) dissolved in toluene (3 mL) were added triethylorthoformate (3.0 mL) and *p*-toluenesulfonic acid (0.2 mmol, 0.1 equiv). The reaction mixture was heated to reflux for 2 h, cooled to r.t., and concentrated. The residue was dissolved in Et_2O and washed with H_2O (2 × 10 mL), 0.1 N HCl (10 mL), and brine (10 mL); dried over Na_2SO_4; filtered; and concentrated. The crude product was purified by column chromatography on silica gel to afford compound **23** as a light yellow solid in 65% yield. ^{1}H NMR (400 MHz, $CDCl_3$): δ 8.50 (s, 1H), 8.16−8.08 (m, 2H), 7.64−7.51 (m, 3H), ^{13}C NMR (101 MHz, $CDCl_3$): δ 164.79, 152.63, 132.02, 129.14, 127.12, 123.51, ESI−TOF−HRMS *m/z*: calcd for (M + H) $C_8H_7N_2O$, 147.0553; found, 147.0551.

4.2. Protein Expression and Purification. Full-length human IDO1 gene was cloned into the pET-28a vector and expressed in *E. coli* Rosetta (DE3) cells. Protein was produced in the LB medium supplemented with 0.5 mM dALA (5-aminolevulinic acid) and was induced by addition of 0.1 mM isopropylthio-β-galactoside overnight at 16 °C. The culture was harvested and frozen at −80 °C until further use. The frozen cells were lysed by sonication in 20 mM Tris pH 7, 400 mM NaCl, 1 mM $MgCl_2$, 20 mM imidazole, 1 mM DTT, 0.5 mg/mL lysozyme, and protease inhibitor. After centrifugation, the supernatant was loaded into a HisTrap HP column pre-equilibrated with buffer containing 20 mM Tris pH 7, 500 mM NaCl, and 20 mM imidazole and eluted with the same buffer containing 500 mM imidazole. Fractions containing IDO1 were pooled, concentrated, and injected on a size exclusion chromatography column (HiLoad Superdex S75 16/60) to increase purity. hIDO1 fractions were concentrated to 20 mg/mL in 20 mM Tris pH 7 and 150 mM NaCl.

4.3. Protein Crystallization, Data Collection, Structure Determination, and Model Refinement. hIDO1 protein at 20 mg/mL was mixed with compounds **4f**, **5f**, and **5g** at a final concentration of 5 mM and co-crystallized by a hanging drop vapor diffusion method. Crystals formed in a couple of days in 20% PEG 1500, 0.15 M potassium thiocyanate, and 0.1 M Tris pH 8.5. The crystals were cryoprotected with 25% glycerol. Diffraction data were collected at the Paul Scherrer Institute (SLS, Villigen) at PXII−X10SA beamline. Data were processed with the XDS Program Package.[97] Structures were solved by molecular replacement using Phaser-MR and chain A of PDB entry 2d0t[19] as the model. Manual model building and structure refinement were carried out in Phenix Suite[98] using coot[99] software and phenix-refine, respectively. After validation, ligand-bound IDO1 models were deposited in the PDB database under PDB codes 7ah4 (**4f**), 7ah6 (**5f**), and 7ah6 (**5g**). Data collection and refinement statistics are summarized in the Supporting Information (Table S2). The structures were displayed with PyMOL (http://www.pymol.org/) and UCSF Chimera.[100]

4.4. Density Functional Theory Calculations. Quantum chemical geometry optimizations and charge calculations were carried out in the density functional theory (DFT) framework with the PBE0 hybrid functional[101] using the Gaussian09 code.[102] Geometry optimizations were carried out with standard settings and the TZVP basis set,[103] while atomic point charges derived from a Hirshfeld population analysis[104] were calculated with the aug-cc-pVTZ basis set[105−107] to obtain converged charges. We also tested the use of atomic point charges derived from a natural population

analysis, a Mulliken population analysis, a Bader charge analysis, and electrostatic potential-derived charges according to the Merz−Singh−Kollman scheme. Solvation effects were taken into account by the polarizable continuum model[108] as implemented in Gaussian09. The histidine-bound heme complex of IDO1 was modeled by an iron−porphin−imidazole system. Binding energies were calculated by subtracting the energy of the iron−porphin−imidazole system and the energy of the isolated ligand from the energy of the 6-fold coordinated system. For the ferric iron−porphin−imidazole system, the ground state with the hybrid DFT functional PBE0 is a quartet, while for the ferrous system, it is a quintuplet. For the 6-fold coordinated systems, a low-spin complex was always assumed, as it has been found experimentally.[58]

4.5. MM-GBSA Calculations. Starting from the crystal structure 2d0t of the complex between hIDO1 and compound **1a**,[19] we removed chain B, the *N*-cyclohexyltaurine molecules, and the resolved water molecules. For all other compounds, ligand **1a** was replaced by the docked conformation of the respective ligand. A covalent bond with an equilibrium distance of 1.97 Å and a force constant of 250 kcal/mol/Å² was added between the heme iron and the coordinated ligand nitrogen atom. The ligand force fields were generated with the SwissParam algorithm.[109] MD simulations were performed in the CHARMM program[110] version 36b1 with the CHARMM27 force field.[111,112] The systems were locally solvated in a sphere of TIP3P water[113] of 25 Å surrounding the active site using the stochastic boundary method.[114] A time step of 1 fs was used. After 220 ps of initial heating and equilibration, data was collected for 2.5 ns. Structural snapshots excluding water molecules were saved every 10 ps for a total of 250 frames. At least three simulations with independent initial velocities were carried out for each ligand.

In the MM-GBSA approach,[84−86] the binding free energy is written as the sum of the change in gas-phase enthalpy $\Delta H_{bind,gas}$, the solvation free energy ΔG_{solv}, and the entropic contribution $-T\Delta S$.

$$\Delta G_{bind} = \Delta H_{bind,gas} + \Delta G_{solv} - T\Delta S$$

in which

$$\Delta H_{bind,gas} = \Delta H_{elec} + \Delta H_{vdW} + \Delta H_{intra}$$

and

$$\Delta G_{solv} = \Delta G_{solv,elec} + \Delta G_{solv,np} = \Delta G_{solv,elec} + \gamma \Delta SASA$$

where ΔH_{elec} is the electrostatic interaction energy, ΔH_{vdW} is the van der Waals interaction energy, ΔH_{intra} is the change in internal energy of the ligand and the receptor, $\Delta G_{solv,elec}$ is the electrostatic contribution to the solvation free energy, $\Delta G_{solv,np}$ is the non-polar contribution, and SASA is the solvent-accessible surface area. Here, we neglected the entropic term and the change in internal energy. $\Delta G_{solv,elec}$ was calculated with the GB-MV2 model[115,116] and a value of 0.0072 kcal/mol/Å² was used for the parameter γ.[117,118] For each neutral ligand, the values were averaged over a minimum of 750 structural snapshots extracted from three independent simulations, while for charged ligands, 1500 structural snapshots were extracted from six independent simulations to improve convergence. All ligand interactions with the heme porphyrin ring and the His346 side chain were excluded from the analysis. The standard errors were calculated taking into account the autocorrelation within the data.[119]

4.6. Electrostatic Potential Calculation. Electrostatic potentials were calculated with the UHBD code[120] on the structure of hIDO1 extracted from its complex with compound MMG-0358 in structure 6r63.[15] The protein was described with the CHARMM27 force field,[111,112] and the charge of the iron was left at +0.24 for the ferrous complex and set to +1.24 for the ferric complex.

4.7. Enzymatic Assays. The enzymatic inhibition assays were performed as described by Takikawa *et al.*[121] with some modifications. Briefly, the reaction mixture (100 μL) contained potassium phosphate buffer (100 mM, pH 6.5), ascorbic acid (20 mM), catalase (400 units/mL), methylene blue (10 μM), purified recombinant IDO1 (2.5 ng/μL), L-trp (100 μM), Triton X-100 (0.01%), and DMSO (5 μL). The inhibitors were serially diluted 3-fold for at least eight different

concentrations. After incubation at room temperature for 20 min, the reaction was stopped in its linear phase by addition of trichloroacetic acid solution (40 mL, 30% w/v), and the samples were incubated at 50 °C for 30 min. After centrifugation, 80 μL of supernatant from each well was used for HPLC analysis.

The mobile phase for HPLC analysis was composed of 50% (v/v) of methanol and 50% of sodium citrate buffer (40 mM, pH 2.4) containing 400 μM sodium dodecyl sulfate. An Agilent Zorbax Eclipse XDB C18 column (150 n 4.6 mm) was used at 23 °C with a flow rate of 1 mL/min and an injection volume of 20 μL. For detection of kynurenine, absorption at 365 nm was measured, while the remaining L-trp was detected at a wavelength of 280 nm. All assays were carried out in duplicates. The activity Act of each compound was calculated as Act = $-RT \ln$ IC$_{50}$ in analogy to the relation between the binding free energy and the measured K_i values.

4.8. Cellular Assays. The cDNA encoding hIDO1 (NCBI, NM_0021464.3) was purchased from Origene as a pCMV6-Entry vector (RC206592). The full ORF of hIDO1 was cloned into the mammalian expression vector pcDNA6/myc-His from Invitrogen. Human embryonic kidney 293T (HEK 293T) cells were transiently transfected with the plasmid construct encoding hIDO1. A 75 cm^2 flask containing HEK 293T cells at a confluency of 70% was transfected with the jetPEI DNA transfection reagent (Polyplus transfection) according to manufacturer's protocol. A total of 20 μg of pcDNA-IDO1 along with 5 μg of pcDNA-GFP plasmid was used for the transfection; GFP was used to evaluate the transfection efficiency prior to the cellular assays; 16−18 h post-transfection, the 293T cells were detached with trypsin, centrifuged, and resuspended in 25 mL of DMEM medium without phenol red, supplemented with penicillin and streptomycin, 10% fetal bovine serum, and 1 mM pyruvate (Gibco). Subsequently, 100 μL of cells were distributed to each well of two 96-well round-bottom plates that had been pre-loaded with 100 μL DMEM and the small organic test molecule in DMSO (for a final DMSO concentration of 2%). The DMEM medium contains 78 μM L-trp and was supplemented with 500 μM of L-trp for hIDO1. Cells transfected with hIDO1 were incubated for 7 h at 37 °C in a CO$_2$ incubator. The reaction was stopped in its linear phase by adding trichloroacetic acid (TCA) to the medium at a final concentration of 4%. Plates were centrifuged for 15 min at 4000 rpm. The supernatant (100 μL) was added to 100 μL of 2% (w/v) p-DMAB in glacial acetic acid. After 10 min, the absorbance was measured at a wavelength of 480 nm to detect kynurenine formation.[122] Alternatively, kynurenine content was determined by HPLC as done for the enzymatic assay.

4.9. Cell Viability. Following DMSO (negative control) or inhibitor treatments, apoptotic cells were detected by 4′,6-diamidino-2-phenylindole (DAPI) staining. Briefly, after 7 h of incubation, the cells were washed with PBS, resuspended in PBS with 1 μg/mL of DAPI, and immediately analyzed using a BD LSR II cytometer. A 405 nm laser with a 450/50 nm band-pass filter was used to collect data.

■ ASSOCIATED CONTENT

ⓢ Supporting Information

The Supporting Information is available free of charge at https://pubs.acs.org/doi/10.1021/acs.jmedchem.0c01968.

> Enzymatic and cellular IDO1 inhibition and toxicity data; data collection and refinement statistics for X-ray crystallography; calculated Hirshfeld charges and activity information for scaffolds **7−35**; enzymatic dose−response curves and Hill slopes for compounds **1a−6f**; cellular dose−response curves and Hill slopes for selected compounds; correlation between kynurenine detection by Ehrlich reagent and by HPLC for cellular assays; 2F$_o$ − F$_c$ and F$_o$ − F$_c$ maps for active sites of **4f**, **5f**, and **5g** bound to IDO1; DFT-optimized ligand structures **1a−6f**; correlation between calculated Hirshfeld charge on iron-binding nitrogen atom and experimentally measured activities; DFT-optimized

> structures of ligand/heme models of compounds **1a−6f**; DFT-calculated iron−nitrogen bond lengths including neutral model structures; MM-GBSA results; ^{1}H and ^{13}C NMR spectra for synthesized compounds; and HPLC purity analysis of compound **5f** (PDF)
>
> Molecular formula strings for all compound (CSV)

Accession Codes

IDO1 in complex with compounds **4f** (PDB ID 7ah4), **5f** (7ah5), and **5g** (7ah6). Authors will release the atomic coordinates and experimental data upon article publication.

■ AUTHOR INFORMATION

Corresponding Authors

Ute F. Röhrig − *Molecular Modeling Group, SIB Swiss Institute of Bioinformatics, 1015 Lausanne, Switzerland;* ⓞ orcid.org/0000-0002-4676-4087; Email: Ute.Roehrig@sib.swiss

Olivier Michielin − *Molecular Modeling Group, SIB Swiss Institute of Bioinformatics, 1015 Lausanne, Switzerland; Department of Oncology, Ludwig Cancer Research-Lausanne Branch, University Hospital of Lausanne (CHUV), 1011 Lausanne, Switzerland;* Email: Olivier.Michielin@chuv.ch

Vincent Zoete − *Molecular Modeling Group, SIB Swiss Institute of Bioinformatics, 1015 Lausanne, Switzerland; Department of Oncology UNIL-CHUV, Ludwig Lausanne Branch, University of Lausanne, 1066 Epalinges, Switzerland;* ⓞ orcid.org/0000-0002-2336-6537; Email: Vincent.Zoete@unil.ch

Authors

Somi Reddy Majjigapu − *Molecular Modeling Group, SIB Swiss Institute of Bioinformatics, 1015 Lausanne, Switzerland; Laboratory of Glycochemistry and Asymmetric Synthesis, École Polytechnique Fédérale de Lausanne (EPFL), 1015 Lausanne, Switzerland;* ⓞ orcid.org/0000-0001-6422-5223

Aline Reynaud − *Protein Production and Structure Core Facility, School of Life Sciences, École Polytechnique Fédérale de Lausanne (EPFL), 1015 Lausanne, Switzerland*

Florence Pojer − *Protein Production and Structure Core Facility, School of Life Sciences, École Polytechnique Fédérale de Lausanne (EPFL), 1015 Lausanne, Switzerland*

Nahzli Dilek − *Molecular Modeling Group, SIB Swiss Institute of Bioinformatics, 1015 Lausanne, Switzerland*

Patrick Reichenbach − *Department of Oncology UNIL-CHUV, Ludwig Lausanne Branch, University of Lausanne, 1066 Epalinges, Switzerland*

Kelly Ascencao − *Molecular Modeling Group, SIB Swiss Institute of Bioinformatics, 1015 Lausanne, Switzerland*

Melita Irving − *Department of Oncology UNIL-CHUV, Ludwig Lausanne Branch, University of Lausanne, 1066 Epalinges, Switzerland*

George Coukos − *Department of Oncology UNIL-CHUV, Ludwig Lausanne Branch, University of Lausanne, 1066 Epalinges, Switzerland; Department of Oncology, Ludwig Cancer Research-Lausanne Branch, University Hospital of Lausanne (CHUV), 1011 Lausanne, Switzerland*

Pierre Vogel − *Laboratory of Glycochemistry and Asymmetric Synthesis, École Polytechnique Fédérale de Lausanne (EPFL), 1015 Lausanne, Switzerland*

Complete contact information is available at:
https://pubs.acs.org/10.1021/acs.jmedchem.0c01968

Author Contributions

U.F.R. designed the compounds, performed the enzymatic assays and the HPLC analysis of enzymatic and cellular samples, performed QM and MM-GBSA calculations, determined the X-ray crystallographic protein structures with F.P., analyzed and interpreted the data, and wrote the manuscript. S.M.R. and P.V. planned and carried out chemical synthesis and characterization. A.R. and F.P. performed protein expression and crystallography. N.D., P.R., and K.A. carried out the cellular assays under supervision of M.I. and G.C. O.M. and V.Z. initiated the project and provided critical feedback. V.Z. also provided the MM-GBSA algorithm, contributed to compound design, and edited the manuscript.

Notes

The authors declare no competing financial interest.

■ ABBREVIATIONS

AHR, aryl hydrocarbon receptor; IDO1, indoleamine 2,3-dioxygenase 1; MM-GBSA, molecular mechanics-Generalized Born surface area; p-DMAB, p-dimethylaminobenzaldehyde; QM, quantum mechanical; TDO, tryptophan 2,3-dioxygenase

■ REFERENCES

(1) Garber, K. A new cancer immunotherapy suffers a setback. *Science* **2018**, *360*, 588.

(2) Long, G. V.; Dummer, R.; Hamid, O.; Gajewski, T. F.; Caglevic, C.; Dalle, S.; Arance, A.; Carlino, M. S.; Grob, J.-J.; Kim, T. M.; Demidov, L.; Robert, C.; Larkin, J.; Anderson, J. R.; Maleski, J.; Jones, M.; Diede, S. J.; Mitchell, T. C. Epacadostat plus Pembrolizumab versus Placebo plus Pembrolizumab in Patients with Unresectable or Metastatic Melanoma (ECHO-301/KEYNOTE-252): A Phase 3, Randomised, Double-Blind Study. *Lancet Oncol.* **2019**, *20*, 1083−1097.

(3) van den Eynde, B. J.; van Baren, N.; Baurain, J.-F. Is There a Clinical Future for IDO1 Inhibitors After the Failure of Epacadostat in Melanoma? *Annu. Rev. Canc. Biol.* **2020**, *4*, 241−256.

(4) Opitz, C. A.; Litzenburger, U. M.; Sahm, F.; Ott, M.; Tritschler, I.; Trump, S.; Schumacher, T.; Jestaedt, L.; Schrenk, D.; Weller, M.; Jugold, M.; Guillemin, G. J.; Miller, C. L.; Lutz, C.; Radlwimmer, B.; Lehmann, I.; von Deimling, A.; Wick, W.; Platten, M. An Endogenous Tumour-Promoting Ligand of the Human Aryl Hydrocarbon Receptor. *Nature* **2011**, *478*, 197−203.

(5) Platten, M.; Nollen, E. A. A.; Röhrig, U. F.; Fallarino, F.; Opitz, C. A. Tryptophan Metabolism as a Common Therapeutic Target in Cancer, Neurodegeneration and Beyond. *Nat. Rev. Drug Discovery* **2019**, *18*, 379−401.

(6) Campesato, L. F.; Budhu, S.; Tchaicha, J.; Weng, C.-H.; Gigoux, M.; Cohen, I. J.; Redmond, D.; Mangarin, L.; Pourpe, S.; Liu, C.; Zappasodi, R.; Zamarin, D.; Cavanaugh, J.; Castro, A. C.; Manfredi, M. G.; McGovern, K.; Merghoub, T.; Wolchok, J. D. Blockade of the

AHR Restricts a Treg-Macrophage Suppressive Axis Induced by L-Kynurenine. *Nat. Commun.* **2020**, *11*, 4011.

(7) Sadik, A.; Somarribas Patterson, L. F.; Öztürk, S.; Mohapatra, S. R.; Panitz, V.; Secker, P. F.; Pfänder, P.; Loth, S.; Salem, H.; Prentzell, M. T.; Berdel, B.; Iskar, M.; Faessler, E.; Reuter, F.; Kirst, I.; Kalter, V.; Foerster, K. I.; Jäger, E.; Guevara, C. R.; Sobeh, M.; Hielscher, T.; Poschet, G.; Reinhardt, A.; Hassel, J. C.; Zapatka, M.; Hahn, U.; von Deimling, A.; Hopf, C.; Schlichting, R.; Escher, B. I.; Burhenne, J.; Haefeli, W. E.; Ishaque, N.; Böhme, A.; Schäuble, S.; Thedieck, K.; Trump, S.; Seiffert, M.; Opitz, C. A. IL4I1 Is a Metabolic Immune Checkpoint That Activates the AHR and Promotes Tumor Progression. *Cell* **2020**, *182*, 1252−1270.

(8) Pallotta, M. T.; Orabona, C.; Volpi, C.; Vacca, C.; Belladonna, M. L.; Bianchi, R.; Servillo, G.; Brunacci, C.; Calvitti, M.; Bicciato, S.; Mazza, E. M. C.; Boon, L.; Grassi, F.; Fioretti, M. C.; Fallarino, F.; Puccetti, P.; Grohmann, U. Indoleamine 2,3-Dioxygenase Is a Signaling Protein in Long-Term Tolerance by Dendritic Cells. *Nat. Immunol.* **2011**, *12*, 870−878.

(9) Albini, E.; Rosini, V.; Gargaro, M.; Mondanelli, G.; Belladonna, M. L.; Pallotta, M. T.; Volpi, C.; Fallarino, F.; Macchiarulo, A.; Antognelli, C.; Bianchi, R.; Vacca, C.; Puccetti, P.; Grohmann, U.; Orabona, C. Distinct Roles of Immunoreceptor Tyrosine-Based Motifs in Immunosuppressive Indoleamine 2,3-Dioxygenase 1. *J. Cell Mol. Med.* **2017**, *21*, 165−176.

(10) Albini, E.; Coletti, A.; Greco, F.; Pallotta, M. T.; Mondanelli, G.; Gargaro, M.; Belladonna, M. L.; Volpi, C.; Bianchi, R.; Grohmann, U.; Macchiarulo, A.; Orabona, C. Identification of a 2-Propanol Analogue Modulating the Non-Enzymatic Function of Indoleamine 2,3-Dioxygenase 1. *Biochem. Pharmacol.* **2018**, *158*, 286−297.

(11) Nelp, M. T.; Kates, P. A.; Hunt, J. T.; Newitt, J. A.; Balog, A.; Maley, D.; Zhu, X.; Abell, L.; Allentoff, A.; Borzilleri, R.; Lewis, H. A.; Lin, Z.; Seitz, S. P.; Yan, C.; Groves, J. T. Immune-Modulating Enzyme Indoleamine 2,3-Dioxygenase Is Effectively Inhibited by Targeting Its Apo-Form. *Proc. Natl. Acad. Sci. U.S.A.* **2018**, *115*, 3249−3254.

(12) Lim, Y. J.; Foo, T. C.; Yeung, A. W. S.; Tu, X.; Ma, Y.; Hawkins, C. L.; Witting, P. K.; Jameson, G. N. L.; Terentis, A. C.; Thomas, S. R. Human Indoleamine 2,3-Dioxygenase 1 Is an Efficient Mammalian Nitrite Reductase. *Biochemistry* **2019**, *58*, 974−986.

(13) Stanley, C. P.; Maghzal, G. J.; Ayer, A.; Talib, J.; Giltrap, A. M.; Shengule, S.; Wolhuter, K.; Wang, Y.; Chadha, P.; Suarna, C.; Prysyazhna, O.; Scotcher, J.; Dunn, L. L.; Prado, F. M.; Nguyen, N.; Odiba, J. O.; Baell, J. B.; Stasch, J.-P.; Yamamoto, Y.; di Mascio, P.; Eaton, P.; Payne, R. J.; Stocker, R. Singlet Molecular Oxygen Regulates Vascular Tone and Blood Pressure in Inflammation. *Nature* **2019**, *566*, 548−552.

(14) Nelp, M. T.; Zheng, V.; Davis, K. M.; Stiefel, K. J. E.; Groves, J. T. Potent Activation of Indoleamine 2,3-Dioxygenase by Polysulfides. *J. Am. Chem. Soc.* **2019**, *141*, 15288−15300.

(15) Röhrig, U. F.; Reynaud, A.; Majjigapu, S. R.; Vogel, P.; Pojer, F.; Zoete, V. Inhibition Mechanisms of Indoleamine 2,3-Dioxygenase 1 (IDO1). *J. Med. Chem.* **2019**, *62*, 8784−8795.

(16) Ortiz-Meoz, R.; Wang, L.; Matico, R.; Rutkowska, A.; De la Rosa, M.; Bedard, S.; Midgett, R.; Strohmer, K.; Thomson, D.; Zhang, C.; Guss, J.; Totoritis, R.; Consler, T.; Campobasso, N.; Taylor, D.; Lewis, T.; Weaver, K.; Mulbaier, M.; Seal, J.; Dunham, R.; Kazmierski, W.; Favre, D.; Bergamini, G.; Shewchuk, L.; Rendina, A.; Zhang, G. Characterization of Novel Inhibition of Indoleamine 2,3-Dioxygenase by Targeting Its Apo Form. **2018**, bioRxiv:324947.

(17) Röhrig, U. F.; Awad, L.; Grosdidier, A.; Larrieu, P.; Stroobant, V.; Colau, D.; Cerundolo, V.; Simpson, A. J.; Vogel, P.; van den Eynde, B. J.; Zoete, V.; Michielin, O. Rational Design of Indoleamine 2,3-Dioxygenase Inhibitors. *J. Med. Chem.* **2010**, *53*, 1172−1189.

(18) Sono, M. Enzyme Kinetic and Spectroscopic Studies of Inhibitor and Effector Interactions with Indoleamine 2,3-Dioxygenase. 2. Evidence for the Existence of Another Binding Site in the Enzyme for Indole Derivative Effectors. *Biochemistry* **1989**, *28*, 5400−5407.

(19) Sugimoto, H.; Oda, S.-i.; Otsuki, T.; Hino, T.; Yoshida, T.; Shiro, Y. Crystal Structure of Human Indoleamine 2,3-Dioxygenase:

Catalytic Mechanism of O2 Incorporation by a Heme-Containing Dioxygenase. *Proc. Natl. Acad. Sci. U.S.A.* **2006**, *103*, 2611−2616.

(20) Kumar, S.; Jaller, D.; Patel, B.; LaLonde, J. M.; DuHadaway, J. B.; Malachowski, W. P.; Prendergast, G. C.; Muller, A. J. Structure Based Development of Phenylimidazole-Derived Inhibitors of Indoleamine 2,3-Dioxygenase. *J. Med. Chem.* **2008**, *51*, 4968−4977.

(21) Kumar, S.; Waldo, J. P.; Jaipuri, F. A.; Marcinowicz, A.; van Allen, C.; Adams, J.; Kesharwani, T.; Zhang, X.; Metz, R.; Oh, A. J.; Harris, S. F.; Mautino, M. R. Discovery of Clinical Candidate (1R,4r)-4-((R)-2-((S)-6-Fluoro-5H-Imidazo[5,1-a]Isoindol-5-Yl)-1-Hydroxyethyl)Cyclohexan-1-Ol (Navoximod), a Potent and Selective Inhibitor of Indoleamine 2,3-Dioxygenase 1. *J. Med. Chem.* **2019**, *62*, 6705−6733.

(22) Peng, Y.-H.; Ueng, S.-H.; Tseng, C.-T.; Hung, M.-S.; Song, J.-S.; Wu, J.-S.; Liao, F.-Y.; Fan, Y.-S.; Wu, M.-H.; Hsiao, W.-C.; Hsueh, C.-C.; Lin, S.-Y.; Cheng, C.-Y.; Tu, C.-H.; Lee, L.-C.; Cheng, M.-F.; Shia, K.-S.; Shih, C.; Wu, S.-Y. Important Hydrogen Bond Networks in Indoleamine 2,3-Dioxygenase 1 (IDO1) Inhibitor Design Revealed by Crystal Structures of Imidazoleisoindole Derivatives with IDO1. *J. Med. Chem.* **2016**, *59*, 282−293.

(23) Fallarini, S.; Massarotti, A.; Gesù, A.; Giovarruscio, S.; Coda Zabetta, G.; Bergo, R.; Giannelli, B.; Brunco, A.; Lombardi, G.; Sorba, G.; Pirali, T. In silico-driven multicomponent synthesis of 4,5- and 1,5-disubstituted imidazoles as indoleamine 2,3-dioxygenase inhibitors. *MedChemComm* **2016**, *7*, 409−419.

(24) Zou, Y.; Wang, F.; Wang, Y.; Sun, Q.; Hu, Y.; Li, Y.; Liu, W.; Guo, W.; Huang, Z.; Zhang, Y.; Xu, Q.; Lai, Y. Discovery of Imidazoleisoindole Derivatives as Potent IDO1 Inhibitors: Design, Synthesis, Biological Evaluation and Computational Studies. *Eur. J. Med. Chem.* **2017**, *140*, 293−304.

(25) Brant, M. G.; Goodwin-Tindall, J.; Stover, K. R.; Stafford, P. M.; Wu, F.; Meek, A. R.; Schiavini, P.; Wohnig, S.; Weaver, D. F. Identification of Potent Indoleamine 2,3-Dioxygenase 1 (IDO1) Inhibitors Based on a Phenylimidazole Scaffold. *ACS Med. Chem. Lett.* **2018**, *9*, 131−136.

(26) Wen, H.; Liu, Y.; Wang, S.; Wang, T.; Zhang, G.; Chen, X.; Li, Y.; Cui, H.; Lai, F.; Sheng, L. Design and Synthesis of Indoleamine 2,3-Dioxygenase 1 Inhibitors and Evaluation of Their Use as Anti-Tumor Agents. *Molecules* **2019**, *24*, 2124.

(27) Tu, W.; Yang, F.; Xu, G.; Chi, J.; Liu, Z.; Peng, W.; Hu, B.; Zhang, L.; Wan, H.; Yu, N.; Jin, F.; Hu, Q.; Zhang, L.; He, F.; Tao, W. Discovery of Imidazoisoindole Derivatives as Highly Potent and Orally Active Indoleamine-2,3-Dioxygenase Inhibitors. *ACS Med. Chem. Lett.* **2019**, *10*, 949−953.

(28) Bai, Z.; Huang, H.; Chen, J.; Zhang, X.; Ding, Y. Identification of novel imidazoles as IDO1 inhibitors through microwave-assisted one-pot multicomponent reactions. *Arch. Pharm.* **2019**, *352*, 1900165.

(29) Serafini, M.; Torre, E.; Aprile, S.; Grosso, E. D.; Gesù, A.; Griglio, A.; Colombo, G.; Travelli, C.; Paiella, S.; Adamo, A.; Orecchini, E.; Coletti, A.; Pallotta, M. T.; Ugel, S.; Massarotti, A.; Pirali, T.; Fallarini, S. Discovery of Highly Potent Benzimidazole Derivatives as Indoleamine 2,3-Dioxygenase-1 (IDO1) Inhibitors: From Structure-Based Virtual Screening to in Vivo Pharmacodynamic Activity. *J. Med. Chem.* **2020**, *63*, 3047−3065.

(30) Tojo, S.; Kohno, T.; Tanaka, T.; Kamioka, S.; Ota, Y.; Ishii, T.; Kamimoto, K.; Asano, S.; Isobe, Y. Crystal Structures and Structure-Activity Relationships of Imidazothiazole Derivatives as IDO1 Inhibitors. *ACS Med. Chem. Lett.* **2014**, *5*, 1119−1123.

(31) Griglio, A.; Torre, E.; Serafini, M.; Bianchi, A.; Schmid, R.; Coda Zabetta, G.; Massarotti, A.; Sorba, G.; Pirali, T.; Fallarini, S. A Multicomponent Approach in the Discovery of Indoleamine 2,3-Dioxygenase 1 Inhibitors: Synthesis, Biological Investigation and Docking Studies. *Bioorg. Med. Chem. Lett.* **2018**, *28*, 651−657.

(32) Serafini, M.; Torre, E.; Aprile, S.; Massarotti, A.; Fallarini, S.; Pirali, T. Synthesis, Docking and Biological Evaluation of a Novel Class of Imidazothiazoles as IDO1 Inhibitors. *Molecules* **2019**, *24*, 1874.

(33) Peng, Y.-H.; Liao, F.-Y.; Tseng, C.-T.; Kuppusamy, R.; Li, A.-S.; Chen, C.-H.; Fan, Y.-S.; Wang, S.-Y.; Wu, M.-H.; Hsueh, C.-C.;

Chang, J.-Y.; Lee, L.-C.; Shih, C.; Shia, K.-S.; Yeh, T.-K.; Hung, M.-S.; Kuo, C.-C.; Song, J.-S.; Wu, S.-Y.; Ueng, S.-H. Unique Sulfur-Aromatic Interactions Contribute to the Binding of Potent Imidazothiazole Indoleamine 2,3-Dioxygenase Inhibitors. *J. Med. Chem.* **2020**, *63*, 1642−1659.

(34) Yue, E. W.; Douty, B.; Wayland, B.; Bower, M.; Liu, X.; Leffet, L.; Wang, Q.; Bowman, K. J.; Hansbury, M. J.; Liu, C.; Wei, M.; Li, Y.; Wynn, R.; Burn, T. C.; Koblish, H. K.; Fridman, J. S.; Metcalf, B.; Scherle, P. A.; Combs, A. P. Discovery of Potent Competitive Inhibitors of Indoleamine 2,3-Dioxygenase with in Vivo Pharmacodynamic Activity and Efficacy in a Mouse Melanoma Model. *J. Med. Chem.* **2009**, *52*, 7364−7367.

(35) Yue, E. W.; Sparks, R.; Polam, P.; Modi, D.; Douty, B.; Wayland, B.; Glass, B.; Takvorian, A.; Glenn, J.; Zhu, W.; Bower, M.; Liu, X.; Leffet, L.; Wang, Q.; Bowman, K. J.; Hansbury, M. J.; Wei, M.; Li, Y.; Wynn, R.; Burn, T. C.; Koblish, H. K.; Fridman, J. S.; Emm, T.; Scherle, P. A.; Metcalf, B.; Combs, A. P. INCB24360 (Epacadostat), a Highly Potent and Selective Indoleamine-2,3-Dioxygenase 1 (IDO1) Inhibitor for Immuno-Oncology. *ACS Med. Chem. Lett.* **2017**, *8*, 486−491.

(36) Wu, Y.; Xu, T.; Liu, J.; Ding, K.; Xu, J. Structural Insights into the Binding Mechanism of IDO1 with Hydroxylamidine Based Inhibitor INCB14943. *Biochem. Biophys. Res. Commun.* **2017**, *487*, 339−343.

(37) Lewis-Ballester, A.; Pham, K. N.; Batabyal, D.; Karkashon, S.; Bonanno, J. B.; Poulos, T. L.; Yeh, S.-R. Structural Insights into Substrate and Inhibitor Binding Sites in Human Indoleamine 2,3-Dioxygenase 1. *Nat. Commun.* **2017**, *8*, 1693.

(38) Luo, S.; Xu, K.; Xiang, S.; Chen, J.; Chen, C.; Guo, C.; Tong, Y.; Tong, L. High-Resolution Structures of Inhibitor Complexes of Human Indoleamine 2,3-Dioxygenase 1 in a New Crystal Form. *Acta Crystallogr., Sect. F: Struct. Biol. Commun.* **2018**, *74*, 717−724.

(39) Zhang, H.; Liu, K.; Pu, Q.; Achab, A.; Ardolino, M. J.; Cheng, M.; Deng, Y.; Doty, A. C.; Ferguson, H.; Fradera, X.; Knemeyer, I.; Kurukulasuriya, R.; Lam, Y.-h.; Lesburg, C. A.; Martinot, T. A.; McGowan, M. A.; Miller, J. R.; Otte, K.; Biju, P. J.; Sciammetta, N.; Solban, N.; Yu, W.; Zhou, H.; Wang, X.; Bennett, D. J.; Han, Y. Discovery of Amino-Cyclobutarene-Derived Indoleamine-2,3-Dioxygenase 1 (IDO1) Inhibitors for Cancer Immunotherapy. *ACS Med. Chem. Lett.* **2019**, *10*, 1530−1536.

(40) Röhrig, U. F.; Zoete, V.; Michielin, O. The Binding Mode of N-Hydroxyamidines to Indoleamine 2,3-Dioxygenase 1 (IDO1). *Biochemistry* **2017**, *56*, 4323−4325.

(41) Paul, S.; Roy, A.; Deka, S. J.; Panda, S.; Trivedi, V.; Manna, D. Nitrobenzofurazan derivatives of N′-hydroxyamidines as potent inhibitors of indoleamine-2,3-dioxygenase 1. *Eur. J. Med. Chem.* **2016**, *121*, 364−375.

(42) Du, Q.; Feng, X.; Wang, Y.; Xu, X.; Zhang, Y.; Qu, X.; Li, Z.; Bian, J. Discovery of Phosphonamidate IDO1 Inhibitors for the Treatment of Non-Small Cell Lung Cancer. *Eur. J. Med. Chem.* **2019**, *182*, 111629.

(43) Chen, S.; Guo, W.; Liu, X.; Sun, P.; Wang, Y.; Ding, C.; Meng, L.; Zhang, A. Design, Synthesis and Antitumor Study of a Series of N-Cyclic Sulfamoylaminoethyl Substituted 1,2,5-Oxadiazol-3-Amines as New Indoleamine 2, 3-Dioxygenase 1 (IDO1) Inhibitors. *Eur. J. Med. Chem.* **2019**, *179*, 38−55.

(44) Song, X.; Sun, P.; Wang, J.; Guo, W.; Wang, Y.; Meng, L.-h.; Liu, H. Design, Synthesis, and Biological Evaluation of 1,2,5-Oxadiazole-3-Carboximidamide Derivatives as Novel Indoleamine-2,3-Dioxygenase 1 Inhibitors. *Eur. J. Med. Chem.* **2020**, *189*, 112059.

(45) Steeneck, C.; Kinzel, O.; Anderhub, S.; Hornberger, M.; Pinto, S.; Morschhaeuser, B.; Braun, F.; Kleymann, G.; Hoffmann, T. Discovery of Hydroxyamidine Based Inhibitors of IDO1 for Cancer Immunotherapy with Reduced Potential for Glucuronidation. *ACS Med. Chem. Lett.* **2020**, *11*, 179−187.

(46) Qian, S.; He, T.; Wang, W.; He, Y.; Zhang, M.; Yang, L.; Li, G.; Wang, Z. Discovery and preliminary structure-activity relationship of 1H-indazoles with promising indoleamine-2,3-dioxygenase 1 (IDO1) inhibition properties. *Bioorg. Med. Chem.* **2016**, *24*, 6194−6205.

(47) Pradhan, N.; Paul, S.; Deka, S. J.; Roy, A.; Trivedi, V.; Manna, D. Identification of Substituted 1H-Indazoles as Potent Inhibitors for Immunosuppressive Enzyme Indoleamine 2,3-Dioxygenase 1. *ChemistrySelect* **2017**, *2*, 5511−5517.

(48) Tsujino, H.; Uno, T.; Yamashita, T.; Katsuda, M.; Takada, K.; Saiki, T.; Maeda, S.; Takagi, A.; Masuda, S.; Kawano, Y.; Meguro, K.; Akai, S. Correlation of Indoleamine-2,3-Dioxigenase 1 Inhibitory Activity of 4,6-Disubstituted Indazole Derivatives and Their Heme Binding Affinity. *Bioorg. Med. Chem. Lett.* **2019**, *29*, 126607.

(49) Yang, L.; Chen, Y.; He, J.; Njoya, E. M.; Chen, J.; Liu, S.; Xie, C.; Huang, W.; Wang, F.; Wang, Z.; Li, Y.; Qian, S. 4,6-Substituted-1H-Indazoles as Potent IDO1/TDO Dual Inhibitors. *Bioorg. Med. Chem.* **2019**, *27*, 1087−1098.

(50) Röhrig, U. F.; Majjigapu, S. R.; Grosdidier, A.; Bron, S.; Stroobant, V.; Pilotte, L.; Colau, D.; Vogel, P.; van den Eynde, B. J.; Zoete, V.; Michielin, O. Rational Design of 4-Aryl-1,2,3-Triazoles for Indoleamine 2,3-Dioxygenase 1 Inhibition. *J. Med. Chem.* **2012**, *55*, 5270−5290.

(51) Alexandre, J. A. C.; Swan, M. K.; Latchem, M. J.; Boyall, D.; Pollard, J. R.; Hughes, S. W.; Westcott, J. New 4-Amino-1,2,3-Triazole Inhibitors of Indoleamine 2,3-Dioxygenase Form a Long-Lived Complex with the Enzyme and Display Exquisite Cellular Potency. *ChemBioChem* **2018**, *19*, 552−561.

(52) Panda, S.; Pradhan, N.; Chatterjee, S.; Morla, S.; Saha, A.; Roy, A.; Kumar, S.; Bhattacharyya, A.; Manna, D. 4,5-Disubstituted 1,2,3-Triazoles: Effective Inhibition of Indoleamine 2,3-Dioxygenase 1 Enzyme Regulates T Cell Activity and Mitigates Tumor Growth. *Sci. Rep.* **2019**, *9*, 18455.

(53) Petrunak, E. M.; Rogers, S. A.; Aubé, J.; Scott, E. E. Structural and Functional Evaluation of Clinically Relevant Inhibitors of Steroidogenic Cytochrome P450 17A1. *Drug Metab. Dispos.* **2017**, *45*, 635−645.

(54) Röhrig, U. F.; Majjigapu, S. R.; Chambon, M.; Bron, S.; Pilotte, L.; Colau, D.; van den Eynde, B. J.; Turcatti, G.; Vogel, P.; Zoete, V.; Michielin, O. Detailed Analysis and Follow-up Studies of a High-Throughput Screening for Indoleamine 2,3-Dioxygenase 1 (IDO1) Inhibitors. *Eur. J. Med. Chem.* **2014**, *84*, 284−301.

(55) Meininger, D.; Zalameda, L.; Liu, Y.; Stepan, L. P.; Borges, L.; McCarter, J. D.; Sutherland, C. L. Purification and Kinetic Characterization of Human Indoleamine 2,3-Dioxygenases 1 and 2 (IDO1 and IDO2) and Discovery of Selective IDO1 Inhibitors. *Biochim. Biophys. Acta, Proteins Proteomics* **2011**, *1814*, 1947−1954.

(56) Hargrove, T. Y.; Friggeri, L.; Wawrzak, Z.; Qi, A.; Hoekstra, W. J.; Schotzinger, R. J.; York, J. D.; Guengerich, F. P.; Lepesheva, G. I. Structural analyses of Candida albicans sterol 14α-demethylase complexed with azole drugs address the molecular basis of azole-mediated inhibition of fungal sterol biosynthesis. *J. Biol. Chem.* **2017**, *292*, 6728−6743.

(57) Hoekstra, W. J.; Garvey, E. P.; Moore, W. R.; Rafferty, S. W.; Yates, C. M.; Schotzinger, R. J. Design and Optimization of Highly-Selective Fungal CYP51 Inhibitors. *Bioorg. Med. Chem. Lett.* **2014**, *24*, 3455−3458.

(58) Sono, M.; Cady, S. G. Enzyme Kinetic and Spectroscopic Studies of Inhibitor and Effector Interactions with Indoleamine 2,3-Dioxygenase. 1. Norharman and 4-Phenylimidazole Binding to the Enzyme as Inhibitors and Heme Ligands. *Biochemistry* **1989**, *28*, 5392−5399.

(59) Mautino, M. R.; Kumar, S.; Jaipuri, F.; Waldo, J.; Kesharwani, T.; Zhang, X. Imidazole Derivatives as IDO Inhibitors, WO/2011/056652. WO2011056652A1, 2011.

(60) Bondy, S. S.; Cannizzaro, C. E.; Chien-Hung, C.; Link, J. O.; Qui, L.; Schroeder, S. D.; Winston, T. C.; Zhang, J. 5-Membered Heteroaryls and Their Use as Antiviral Agents, WO/2014/110298. WO2014110298A1, 2014.

(61) Pratt, D. A.; Pesavento, R. P.; van der Donk, W. A. Model Studies of the Histidine-Tyrosine Cross-Link in CytochromecOxidase Reveal the Flexible Substituent Effect of the Imidazole Moiety. *Org. Lett.* **2005**, *7*, 2735−2738.

(62) Haddach, M.; Tran, J. A.; Pierre, F.; Regan, C. F.; Raffaele, N. B.; Ravula, S.; Ryckman, D. M. Pyrazolopyrimidines and Related Heterocycles as CK2 Inhibitors, WO/2011/068667. WO2011068667A1, 2011.

(63) Sun, X.; Hong, Z.; Liu, M.; Guo, S.; Yang, D.; Wang, Y.; Lan, T.; Gao, L.; Qi, H.; Gong, P.; Liu, Y. Design, Synthesis, and Biological Activity of Novel Tetrahydropyrazolopyridone Derivatives as FXa Inhibitors with Potent Anticoagulant Activity. *Bioorg. Med. Chem.* **2017**, *25*, 2800−2810.

(64) Xie, F.; Du, C.-C.; Dong, J.-L.; Du, J.-Q.; Han, Y.-Z.; Wang, D.-Z. New Complexes Constructed Based on (1H-Tetrazol-5-Yl)Phenol: Synthesis, Structures and Properties. *Polyhedron* **2018**, *149*, 17−24.

(65) Xu, Z.-L.; Li, H.-X.; Ren, Z.-G.; Du, W.-Y.; Xu, W.-C.; Lang, J.-P. Cu(OAc)2·H2O-catalyzed N-arylation of nitrogen-containing heterocycles. *Tetrahedron* **2011**, *67*, 5282−5288.

(66) Pedras, M. S. C.; Suchy, M. Design, Synthesis, and Antifungal Activity of Inhibitors of Brassilexin Detoxification in the Plant Pathogenic Fungus Leptosphaeria Maculans. *Bioorg. Med. Chem.* **2006**, *14*, 714−723.

(67) Aoyama, T.; Iwamoto, Y.; Shioiri, T. New Methods and Reagents in Organic Synthesis. 59. Lithium Trimethylsilydiazomethane: A New Synthon for the Preparation of 5-Substituted 1,2,3-Thiadiazoles. *Heterocycles* **1986**, *24*, 589−592.

(68) Yamamuro, D.; Uchida, R.; Ohtawa, M.; Arima, S.; Futamura, Y.; Katane, M.; Homma, H.; Nagamitsu, T.; Osada, H.; Tomoda, H. Synthesis and Biological Activity of 5-(4-Methoxyphenyl)-Oxazole Derivatives. *Bioorg. Med. Chem. Lett.* **2015**, *25*, 313−316.

(69) Wakefield, B. J. Product Class 9: Isoxazoles. In *Science of Synthesis*; Schaumann, E., Ed.; Thieme Verlagsgruppe: Stuttgart, New York, Delhi, Rio, 2002; pp 229−288.

(70) Ohmoto, K.; Yamamoto, T.; Okuma, M.; Horiuchi, T.; Imanishi, H.; Odagaki, Y.; Kawabata, K.; Sekioka, T.; Hirota, Y.; Matsuoka, S.; Nakai, H.; Toda, M.; Cheronis, J. C.; Spruce, L. W.; Gyorkos, A.; Wieczorek, M. Development of Orally Active Non-peptidic Inhibitors of Human Neutrophil Elastase. *J. Med. Chem.* **2001**, *44*, 1268−1285.

(71) Röhrig, U. F.; Majjigapu, S. R.; Vogel, P.; Zoete, V.; Michielin, O. Challenges in the Discovery of Indoleamine 2,3-Dioxygenase 1 (IDO1) Inhibitors. *J. Med. Chem.* **2015**, *58*, 9421−9437.

(72) Morrison, J. F. Kinetics of the Reversible Inhibition of Enzyme-Catalysed Reactions by Tight-Binding Inhibitors. *Biochim. Biophys. Acta, Enzymol.* **1969**, *185*, 269−286.

(73) Kuzmič, P. History, Variants and Usage of the "Morrison Equation" in Enzyme Inhibition Kinetics. *BioKin Technical Note*; BioKin Ltd., 2015; pp 1−15.

(74) Wilcken, R.; Zimmermann, M. O.; Lange, A.; Zahn, S.; Kirchner, B.; Boeckler, F. M. Addressing Methionine in Molecular Design through Directed Sulfur-Halogen Bonds. *J. Chem. Theory Comput.* **2011**, *7*, 2307−2315.

(75) Wilcken, R.; Zimmermann, M. O.; Lange, A.; Joerger, A. C.; Boeckler, F. M. Principles and Applications of Halogen Bonding in Medicinal Chemistry and Chemical Biology. *J. Med. Chem.* **2013**, *56*, 1363−1388.

(76) Bissantz, C.; Kuhn, B.; Stahl, M. A Medicinal Chemist's Guide to Molecular Interactions. *J. Med. Chem.* **2010**, *53*, 5061−5084.

(77) Shinada, N. K.; de Brevern, A. G.; Schmidtke, P. Halogens in Protein-Ligand Binding Mechanism: A Structural Perspective. *J. Med. Chem.* **2019**, *62*, 9341−9356.

(78) Tomek, P.; Palmer, B. D.; Flanagan, J. U.; Sun, C.; Raven, E. L.; Ching, L.-M. Discovery and Evaluation of Inhibitors to the Immunosuppressive Enzyme Indoleamine 2,3-Dioxygenase 1 (IDO1): Probing the Active Site-Inhibitor Interactions. *Eur. J. Med. Chem.* **2017**, *126*, 983−996.

(79) Onufriev, A. v.; Alexov, E. Protonation and PK Changes in Protein-Ligand Binding. *Q. Rev. Biophys.* **2013**, *46*, 181−209.

(80) George, P.; Hanania, G. I. H.; Irvine, D. H.; Abu-Issa, I. 1090. The effect of co-ordination on ionization. Part IV. Imidazole and its ferrimyoglobin complex. *J. Chem. Soc.* **1964**, 5689−5694.

(81) Song, Y.; Mao, J.; Gunner, M. R. Electrostatic Environment of Hemes in Proteins: pKas of Hydroxyl Ligands†. *Biochemistry* **2006**, *45*, 7949−7958.

(82) Erman, J. E.; Chinchilla, D.; Studer, J.; Vitello, L. B. Binding of Imidazole, 1-Methylimidazole and 4-Nitroimidazole to Yeast Cytochrome c Peroxidase (CcP) and the Distal Histidine Mutant, CcP(H52L). *Biochim. Biophys. Acta, Proteins Proteomics* **2015**, *1854*, 869−881.

(83) Schofield, K.; Grimmett, M. R.; Keene, B. R. T. *Heteroaromatic Nitrogen Compounds: The Azoles*; Cambridge University Press: Cambridge [England], 1976.

(84) Srinivasan, J.; Cheatham, T. E.; Cieplak, P.; Kollman, P. A.; Case, D. A. Continuum Solvent Studies of the Stability of DNA, RNA, and Phosphoramidate−DNA Helices. *J. Am. Chem. Soc.* **1998**, *120*, 9401−9409.

(85) Zoete, V.; Irving, M. B.; Michielin, O. MM-GBSA Binding Free Energy Decomposition and T Cell Receptor Engineering. *J. Mol. Recognit.* **2010**, *23*, 142−152.

(86) Wang, E.; Sun, H.; Wang, J.; Wang, Z.; Liu, H.; Zhang, J. Z. H.; Hou, T. End-Point Binding Free Energy Calculation with MM/PBSA and MM/GBSA: Strategies and Applications in Drug Design. *Chem. Rev.* **2019**, *119*, 9478−9508.

(87) Beers, S.; Xia, C.; Brooks, J.; Kottas, G. Cyclometallated Tetradentate Pt(Ii) Complexes Comprised of One or Two Imidazole Rings with Twisted Aryl Group Bonded to N-1, JP/2013/079235. JP2013079235A, 2013.

(88) Yang, J.; Chen, C.; Tang, X. Cholesterol-Modified Caged SiRNAs for Photoregulating Exogenous and Endogenous Gene Expression. *Bioconjugate Chem.* **2018**, *29*, 1010−1015.

(89) Bellina, F.; Cauteruccio, S.; di Fiore, A.; Rossi, R. Regioselective Synthesis of 4,5-Diaryl-1-methyl-1H-imidazoles Including Highly Cytotoxic Derivatives by Pd-Catalyzed Direct C-5 Arylation of 1-Methyl-1H-imidazole with Aryl Bromides. *Eur. J. Org Chem.* **2008**, 5436−5445.

(90) Kirsch, P.; Jakob, V.; Oberhausen, K.; Stein, S. C.; Cucarro, I.; Schulz, T. F.; Empting, M. Fragment-Based Discovery of a Qualified Hit Targeting the Latency-Associated Nuclear Antigen of the Oncogenic Kaposi's Sarcoma-Associated Herpesvirus/Human Herpesvirus 8. *J. Med. Chem.* **2019**, *62*, 3924−3939.

(91) Strehlke, P. Antifungal Imidazole Derivatives. II. Ethers of (1-Imidazolyl)-Phenols. *Eur. J. Med. Chem.* **1979**, *14*, 227−230.

(92) Shechter, S.; Kauffmann, M.; Sandanyaka, V. P.; Shacham, S. Nuclear Transport Modulators and Uses Thereof, WO/2011/109799. WO2011109799A1, 2011.

(93) Pagacz-Kostrzewa, M.; Sałdyka, M.; Wierzejewska, M.; Khomenko, D. M.; Doroschuk, R. O. Theoretical DFT and Matrix Isolation FTIR Studies of 2-(1,2,4-Triazolyl)Phenol Isomers. *Chem. Phys. Lett.* **2016**, *657*, 156−161.

(94) Knust, H.; Thomas, A. W. Substituted Imidazo[1,5-A][1,2,4]Triazolo[1,5-D][1,4]Benzodiazepine Derivatives. U.S. Patent 0,084,642 A1, 2006.

(95) Treitler, D. S.; Leung, S.; Lindrud, M. Development and Demonstration of a Safer Protocol for the Synthesis of 5-Aryltetrazoles from Aryl Nitriles. *Org. Process Res. Dev.* **2017**, *21*, 460−467.

(96) Antypenko, O. M.; Kovalenko, S. I.; Karpenko, O. v. Synthesis and hydrolytic cleavage of tetrazolo[1,5-c]quinazolines. *Synth. Commun.* **2016**, *46*, 551−555.

(97) Kabsch, W. XDS. *Acta Crystallogr., Sect. D: Biol. Crystallogr.* **2010**, *66*, 125−132.

(98) Adams, P. D.; Afonine, P. v.; Bunkóczi, G.; Chen, V. B.; Davis, I. W.; Echols, N.; Headd, J. J.; Hung, L.-W.; Kapral, G. J.; Grosse-Kunstleve, R. W.; McCoy, A. J.; Moriarty, N. W.; Oeffner, R.; Read, R. J.; Richardson, D. C.; Richardson, J. S.; Terwilliger, T. C.; Zwart, P. H. PHENIX: a comprehensive Python-based system for macromolecular structure solution. *Acta Crystallogr., Sect. D: Biol. Crystallogr.* **2010**, *66*, 213−221.

(99) Emsley, P.; Lohkamp, B.; Scott, W. G.; Cowtan, K. Features and development ofCoot. *Acta Crystallogr., Sect. D: Biol. Crystallogr.* **2010**, *66*, 486−501.

(100) Pettersen, E. F.; Goddard, T. D.; Huang, C. C.; Couch, G. S.; Greenblatt, D. M.; Meng, E. C.; Ferrin, T. E. UCSF Chimera?A Visualization System for Exploratory Research and Analysis. *J. Comput. Chem.* **2004**, *25*, 1605−1612.

(101) Adamo, C.; Cossi, M.; Barone, V. An Accurate Density Functional Method for the Study of Magnetic Properties: The PBE0 Model. *J. Mol. Struct.: THEOCHEM* **1999**, *493*, 145−157.

(102) Frisch, M. J.; Trucks, G. W.; Schlegel, H. B.; Scuseria, G. E.; Robb, M. A.; Cheeseman, J. R.; Scalmani, G.; Barone, V.; Mennucci, B.; Petersson, G. A.; Nakatsuji, H.; Caricato, M.; Li, X.; Hratchian, H. P.; Izmaylov, A. F.; Bloino, J.; Zheng, G.; Sonnenberg, J. L.; Hada, M.; Ehara, M.; Toyota, K.; Fukuda, R.; Hasegawa, J.; Ishida, M.; Nakajima, T.; Honda, Y.; Kitao, O.; Nakai, H.; Vreven, T.; Montgomery, J. A., Jr; Peralta, J. E.; Ogliaro, F.; Bearpark, M.; Heyd, J. J.; Brothers, E.; Kudin, K. N.; Staroverov, V. N.; Kobayashi, R.; Normand, J.; Raghavachari, K.; Rendell, A.; Burant, J. C.; Iyengar, S. S.; Tomasi, J.; Cossi, M.; Rega, N.; Millam, J. M.; Klene, M.; Knox, J. E.; Cross, J. B.; Bakken, V.; Adamo, C.; Jaramillo, J.; Gomperts, R.; Stratmann, R. E.; Yazyev, O.; Austin, A. J.; Cammi, R.; Pomelli, C.; Ochterski, J. W.; Martin, R. L.; Morokuma, K.; Zakrzewski, V. G.; Voth, G. A.; Salvador, P.; Dannenberg, J. J.; Dapprich, S.; Daniels, A. D.; Farkas, Ö.; Foresman, J. B.; Ortiz, J. v.; Cioslowski, J.; Fox, D. J. *Gaussian 09* Revision A.1.; Gaussian, Inc., 2009.

(103) Schäfer, A.; Huber, C.; Ahlrichs, R. Fully Optimized Contracted Gaussian Basis Sets of Triple Zeta Valence Quality for Atoms Li to Kr. *J. Chem. Phys.* **1994**, *100*, 5829−5835.

(104) Hirshfeld, F. L. Bonded-Atom Fragments for Describing Molecular Charge Densities. *Theor. Chim. Acta* **1977**, *44*, 129−138.

(105) Dunning, T. H. Gaussian Basis Sets for Use in Correlated Molecular Calculations. I. The Atoms Boron through Neon and Hydrogen. *J. Chem. Phys.* **1989**, *90*, 1007−1023.

(106) Kendall, R. A.; Dunning, T. H.; Harrison, R. J. Electron affinities of the first-row atoms revisited. Systematic basis sets and wave functions. *J. Chem. Phys.* **1992**, *96*, 6796−6806.

(107) Woon, D. E.; Dunning, T. H. Gaussian Basis Sets for Use in Correlated Molecular Calculations. III. The Atoms Aluminum through Argon. *J. Chem. Phys.* **1993**, *98*, 1358−1371.

(108) Tomasi, J.; Mennucci, B.; Cammi, R. Quantum Mechanical Continuum Solvation Models. *Chem. Rev.* **2005**, *105*, 2999−3094.

(109) Zoete, V.; Cuendet, M. A.; Grosdidier, A.; Michielin, O. SwissParam: A Fast Force Field Generation Tool for Small Organic Molecules. *J. Comput. Chem.* **2011**, *32*, 2359−2368.

(110) Brooks, B. R.; Brooks, C. L.; Mackerell, A. D.; Nilsson, L.; Petrella, R. J.; Roux, B.; Won, Y.; Archontis, G.; Bartels, C.; Boresch, S.; Caflisch, A.; Caves, L.; Cui, Q.; Dinner, A. R.; Feig, M.; Fischer, S.; Gao, J.; Hodoscek, M.; Im, W.; Kuczera, K.; Lazaridis, T.; Ma, J.; Ovchinnikov, V.; Paci, E.; Pastor, R. W.; Post, C. B.; Pu, J. Z.; Schaefer, M.; Tidor, B.; Venable, R. M.; Woodcock, H. L.; Wu, X.; Yang, W.; York, D. M.; Karplus, M. CHARMM: The Biomolecular Simulation Program. *J. Comput. Chem.* **2009**, *30*, 1545−1614.

(111) MacKerell, A. D.; Bashford, D.; Bellott, M.; Dunbrack, R. L.; Evanseck, J. D.; Field, M. J.; Fischer, S.; Gao, J.; Guo, H.; Ha, S.; Joseph-McCarthy, D.; Kuchnir, L.; Kuczera, K.; Lau, F. T. K.; Mattos, C.; Michnick, S.; Ngo, T.; Nguyen, D. T.; Prodhom, B.; Reiher, W. E.; Roux, B.; Schlenkrich, M.; Smith, J. C.; Stote, R.; Straub, J.; Watanabe, M.; Wiórkiewicz-Kuczera, J.; Yin, D.; Karplus, M. All-Atom Empirical Potential for Molecular Modeling and Dynamics Studies of Proteins†. *J. Phys. Chem. B* **1998**, *102*, 3586−3616.

(112) Mackerell, A. D.; Feig, M.; Brooks, C. L. Extending the Treatment of Backbone Energetics in Protein Force Fields: Limitations of Gas-Phase Quantum Mechanics in Reproducing Protein Conformational Distributions in Molecular Dynamics Simulations. *J. Comput. Chem.* **2004**, *25*, 1400−1415.

(113) Jorgensen, W. L.; Chandrasekhar, J.; Madura, J. D.; Impey, R. W.; Klein, M. L. Comparison of Simple Potential Functions for Simulating Liquid Water. *J. Chem. Phys.* **1983**, *79*, 926−935.

(114) Brooks, C. L.; Brünger, A.; Karplus, M. Active Site Dynamics in Protein Molecules: A Stochastic Boundary Molecular-Dynamics Approach. *Biopolymers* **1985**, *24*, 843−865.

(115) Lee, M. S.; Salsbury, F. R.; Brooks, C. L. Novel Generalized Born Methods. *J. Chem. Phys.* **2002**, *116*, 10606−10614.

(116) Lee, M. S.; Feig, M.; Salsbury, F. R.; Brooks, C. L. New Analytic Approximation to the Standard Molecular Volume Definition and Its Application to Generalized Born Calculations. *J. Comput. Chem.* **2003**, *24*, 1348−1356.

(117) Still, W. C.; Tempczyk, A.; Hawley, R. C.; Hendrickson, T. Semianalytical Treatment of Solvation for Molecular Mechanics and Dynamics. *J. Am. Chem. Soc.* **1990**, *112*, 6127−6129.

(118) Gohlke, H.; Kiel, C.; Case, D. a. Insights into Protein-Protein Binding by Binding Free Energy Calculation and Free Energy Decomposition for the Ras-Raf and Ras-RalGDS Complexes. *J. Mol. Biol.* **2003**, *330*, 891−913.

(119) Zięba, A.; Ramza, P. Standard Deviation of the Mean of Autocorrelated Observations Estimated with the Use of the Autocorrelation Function Estimated From the Data. *Metrol. Meas. Syst.* **2011**, *18*, 529−542.

(120) Madura, J. D.; Briggs, J. M.; Wade, R. C.; Davis, M. E.; Luty, B. a.; Ilin, A.; Antosiewicz, J.; Gilson, M. K.; Bagheri, B.; Scott, L. R.; McCammon, J. A. Electrostatics and Diffusion of Molecules in Solution: Simulations with the University of Houston Brownian Dynamics Program. *Comput. Phys. Commun.* **1995**, *91*, 57−95.

(121) Takikawa, O.; Kuroiwa, T.; Yamazaki, F.; Kido, R. Mechanism of Interferon-Gamma Action. Characterization of Indoleamine 2,3-Dioxygenase in Cultured Human Cells Induced by Interferon-Gamma and Evaluation of the Enzyme-Mediated Tryptophan Degradation in Its Anticellular Activity. *J. Biol. Chem.* **1988**, *263*, 2041−2048.

(122) Littlejohn, T. K.; Takikawa, O.; Skylas, D.; Jamie, J. F.; Walker, M. J.; Truscott, R. J. W. Expression and Purification of Recombinant Human Indoleamine 2,3-Dioxygenase. *Protein Expression Purif.* **2000**, *19*, 22−29.